Sustainable Engineering Novit
https://www.sciltp.com/journals/sen

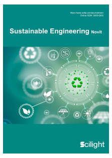

Review

Defects-Engineered Metal-Organic Frameworks for Supercapacitor Platform

Ruiying Fu [1], Lianchao Wang [1], Xutian Yang [1], Chao Li [2,*], Mingjun Ouyang [1], Hua Wu [1], Rui Xi [3,*] and Kuaibing Wang [1,*]

[1] Department of Chemistry, College of Sciences, Nanjing Agricultural University, Nanjing 210095, China
[2] School of Physics and Electronic Engineering, Sichuan University of Science & Engineering, Yibin 644000, China
[3] Department of Applied Chemistry, School of Engineering, The University of Tokyo, 7-3-1 Hongo, Bunkyo-ku, Tokyo 113-8656, Japan
* Correspondence: chaolicc@outlook.com (C.L.); xirui@g.ecc.u-tokyo.ac.jp (R.X.); wangkb@njau.edu.cn (K.W.)

How To Cite: Fu, R.; Wang, L.; Yang, X.; et al. Defects-Engineered Metal-Organic Frameworks for Supercapacitor Platform. *Sustainable Engineering Novit* **2025**, *1*(1), 2. https://doi.org/10.53941/sen.2025.100002.

Received: 30 April 2025
Revised: 14 May 2025
Accepted: 3 June 2025
Published: 8 July 2025

Abstract: The increasing emphasis on eco-friendly energy options has accelerated the use of supercapacitors (SCs) due to their distinct advantages. Nonetheless, they face challenges, such as low power density and high self-discharge rates in practical applications. Metal-organic frameworks (MOFs) have been curated as superior candidate active components for enhancing SC performance stemming from their extensive surface areas, adjustable pore structures, and abundant accessible sites. This paper provides a thorough review of the application of multivariate defect MOFs (MTV-DMOFs) and vacancy engineering in SCs, emphasizing how various defect types (including metal and ligand defects) and their formation processes (such as etching, laser treatment, and pyrolysis) influence electrochemical performance. These defect-engineering strategies have significantly improved the energy density, power density, and cycling stability of SCs.

Keywords: supercapacitors; metal-organic frameworks; defect engineering; energy storage; electrochemical performance

1. Introduction

As humanity advances rapidly, the depletion of fossil fuels and substantial pollution resulting from their combustion have emerged as two critical global challenges. The concepts of ‘carbon peak’ and ‘carbon neutral’ underscore the necessity of advancing green and renewable energy sources [1–4]. Among the various technologies, electrochemical methods offer substantial benefits [5]. First, they eliminate the need for combustion by converting chemical energy into electrical energy through reactions on the electrode surfaces. Second, these processes can be tailored to specific requirements and do not emit pollutants [6–13]. Supercapacitors (SCs) are among the many electrochemical energy storage devices that are extensively utilized owing to their superior power density, long lifespans for charging and discharging, and broad operating temperature range [14–20]. However, in practical applications, SCs encounter challenges such as low power density and high self-discharge rate [21–23]. To overcome these performance limitations, metal-organic framework (MOF) materials have been used [24,25].

MOFs are crystalline porous materials with a periodic network structure formed by the self-assembly of metal nodes with organic ligands via coordination bonds [26–30]. Since Yaghi’s team first identified $Cu(4,4'\text{-}bpy)_{1.5}NO_3(H_2O)_{1.25}$ as a MOF in 1995, these materials have garnered significant attention as an innovative substances [31]. Following the introduction of the MOF-5 prototype, research on novel MOFs has steadily increased [32]. MOFs offer numerous advantages, including adjustable pore sizes [33,34], large specific surface area [35–39], customizable crystal structures [40–43], and numerous active sites [44–46]. These features have facilitated the widespread application of MOFs in various fields, such as hydrogen storage [47–

50], catalysis [51–58], drug delivery [59–63], sensors [64–67], and energy storage [68–72]. In SCs, the exceptionally high characteristic surface area of MOFs affords numerous active sites for charge storage, significantly enhancing these devices' energy density [73–76]. Additionally, a modifiable pore structure is advantageous for rapid ion transport, thereby improving power performance [77,78].

Defect engineering in MOFs is important for changing their structure and function [79]. Introducing defects makes it possible to enhance the material's surface area and porosity while preserving its fundamental properties [80–83]. MOF defects are divided into metal defects [84] and ligand defects [85]. These defects (Figure 1) are not from outside changes or internal instability. They are added on purpose through careful design and control [86–89]. Defect sites in MOFs facilitate guest molecule diffusion through the framework [90,91] and enhance charge transport, making them good for supercapacitors. This review examines the utilization of defective MOFs in supercapacitors to evaluate how structural defects can enhance their performance. Studying the defects in supercapacitors will help future research on innovative supercapacitors with superior energy density and prolonged life, providing better solutions for storing and using green energy.

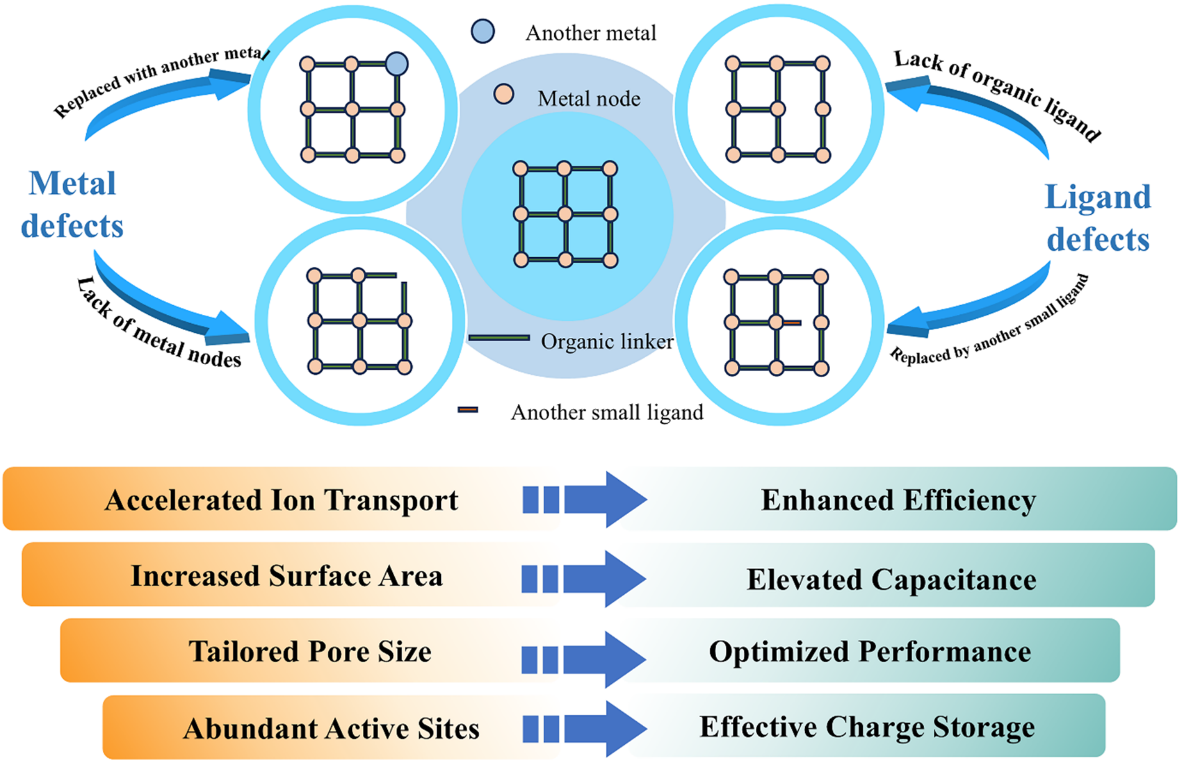

Figure 1. Types of MOF defects and advantages of defective MOFs in SCs.

2. MOFs and Defect Engineering

MOFs can be synthesized using various methods, including solvothermal [92–98], microwave-assisted [99–104], and electrochemical synthesis [105–109]. The synthesis conditions significantly influence the types of defects exhibited by MOFs. These defects arise from misconnections and dislocations before crystallization or splitting after crystallization [110]. Flawless MOFs do not exist, and typical MOFs, such as MOF-5 [111], UiO-66 [112], and MIL-101 [113], inherently possess defects. Wu and colleagues [114] demonstrated that these defects can be intrinsic or intentionally introduced. Recent studies have shown that deliberately introduced defects can impart new functional properties to MOF materials, such as increased catalytic activity [115–119], enhanced adsorption capabilities [120–122], and optimized electrochemical performance [123–126]. Consequently, researchers have intentionally created controllable defects in MOFs using specific techniques to achieve the desired modifications in material properties.

Defective MOF materials in supercapacitors offer distinct advantages, including enhanced electrochemical performance, optimized pore configuration, and improved stability, as illustrated in Figure 1. Various methodologies can be employed to deliberately introduce defects into the MOF lattice, such as metal or non-metal doping, ligand competition, and vacancy engineering. The defects generated by these techniques will be analyzed in the context of specific supercapacitor applications.

3. Defective MOF-Based SCs

SCs offer numerous advantages, including superior power density, high-speed charge, and discharge capabilities, extended cycle life, and excellent safety, thereby increasing their significance in energy-storage systems [127–131]. To boost the electrochemical competence of SCs, various methodologies have been employed, such as the identification of high-performance electrode materials [132–139], incorporation of heteroatom doping [140–142], and design of effective nanostructures [143–147], among others. Although MOFs lack inherent electrochemical advantages, their adjustable properties allow them to be utilized as high-performance electrode materials. By exploiting these defects, MOFs can be designed to address precise application requirements. The significant roles of the various defective MOFs in SCs are explored in detail below.

3.1. Metal-Organic Frameworks with Multiple Defects (MTV-DMOF) in SCs

A promising strategy for synthesizing MOFs is the mixed ligand/metal approach, which can be implemented in two principal ways: first, by directly combining varying quantities of metals or ligands during solvothermal synthesis; and second, through post-synthetic modification techniques [148]. These processes frequently result in specific defects owing to atomic radii or ligand length variations. Particular defective MOFs can be engineered by intentionally incorporating these defect structures. This method of constructing defective MOFs is referred to as Multivariate Defective Metal-Organic Frameworks (MTV-DMOF) (as illustrated in Figure 2a). In the context of synthesizing electrode materials for SCs, the MTV-DMOF approach can significantly enhance the surface characteristics of electrodes. The subsequent discussion explores the applications of MTV-DMOFs in the supercapacitor domain, focusing on two aspects: defect introduction through metal/non-metal doping and ligand competition.

3.1.1. Metal/Non-Metal Doping

In materials research, doping with metals or non-metals is pivotal for enhancing the material properties within the MTV-DMOF framework. This methodology introduces defects in various ways, significantly influencing the microstructure and characteristics of materials. By incorporating metal ions with different radii, lattice stress can be induced, which increases the surface area and active sites and enhances the material's conductivity. These improvements help address low energy density and high self-discharge rates by providing more active sites for charge storage and facilitating faster ion transport [149–151]. For example, Dong and others [149] utilized Fe^{3+} and Fe^{2+} ions to contend with Ni^{2+} ions for coordination during the synthesis of NiFe-MOF. This competition led to the formation of thinner nanosheets and an increase in defects, thereby enhancing the capacitive abilities of the active electrode, as shown in Figure 2b. The optimized NiFe-MOF demonstrated a specific area capacitance of 15.6 F cm^{-2} at 2 mA cm^{-2} and retained 86.3% of its capacitance after 5000 cycles. The irregular supercapacitor constructed with NiFe-MOF achieved an energy-density value of 0.75 mWh cm^{-2} under a power-density value of 8.0 mW cm^{-2}, rendering it an excellent superior-performing energy-storage material.

In a separate study, Patil and colleagues [150] introduced Cu as a dopant into an Fe-based MOF during the synthesis of Cu@Fe-MOF, culminating in the fabrication of a Cu@Fe-MOF/NF thin-film electrode for supercapacitors, as shown in Figure 2c. The incorporation of Cu modified the crystal structure and electron distribution of the original Fe-MOF, which was attributed to the distinct coordination modes and electronic structures of different metal ions, thereby inducing defects within the material. These defects provide additional active sites for the charge storage. At 3 A g^{-1}, the particular capacitance for the Cu@Fe-MOF/NF electrode, characterized by a micron-sized biconical structure, attains 420.54 F g^{-1}, which is twice that of the nano-cubic structure Fe-MOF/NF electrode, measured at 210 F g^{-1}.

Wang et al. [151] synthesized Fe-doped folded Fe/NiS_2 (as depicted in Figure 2d) through a straightforward hydrothermal method combined with an anion exchange approach. The formation of defects is associated with Fe doping because of the difference in the radii of Fe and Ni atoms, which induces local stress variations in the lattice when Fe ions are incorporated into the NiS_2 lattice. Owing to its distinctive two-dimensional structure and the numerous defects introduced by Fe doping, this material parades a huge specific surface area and high conductivity. When the Ni:Fe molar ratio was 1:0.01, $Fe_{0.01}NiS_2$ achieved a particular capacitance of up to 1965.9 F g^{-1} at 0.5 A g^{-1}.

Bu and coworkers [152] successfully synthesized two types of trimetallic sulfides, CNVS and CFVS, which were characterized by a heterogeneous structure, as illustrated in Figure 2e. They employed Co-MOF as the precursor through ion exchange and sulfidation processes. CNVS and CFVS exhibited unique hollow triangular arrays and rich mesoporous structures. Incorporating elements introduces numerous active centers, enhancing the electron and electrolyte transport rates and improving the specific capacitance. Under certain conditions, the specific capacitance reached 6556 mF cm^{-2} for CNVS and 6195 mF cm^{-2} for CFVS.

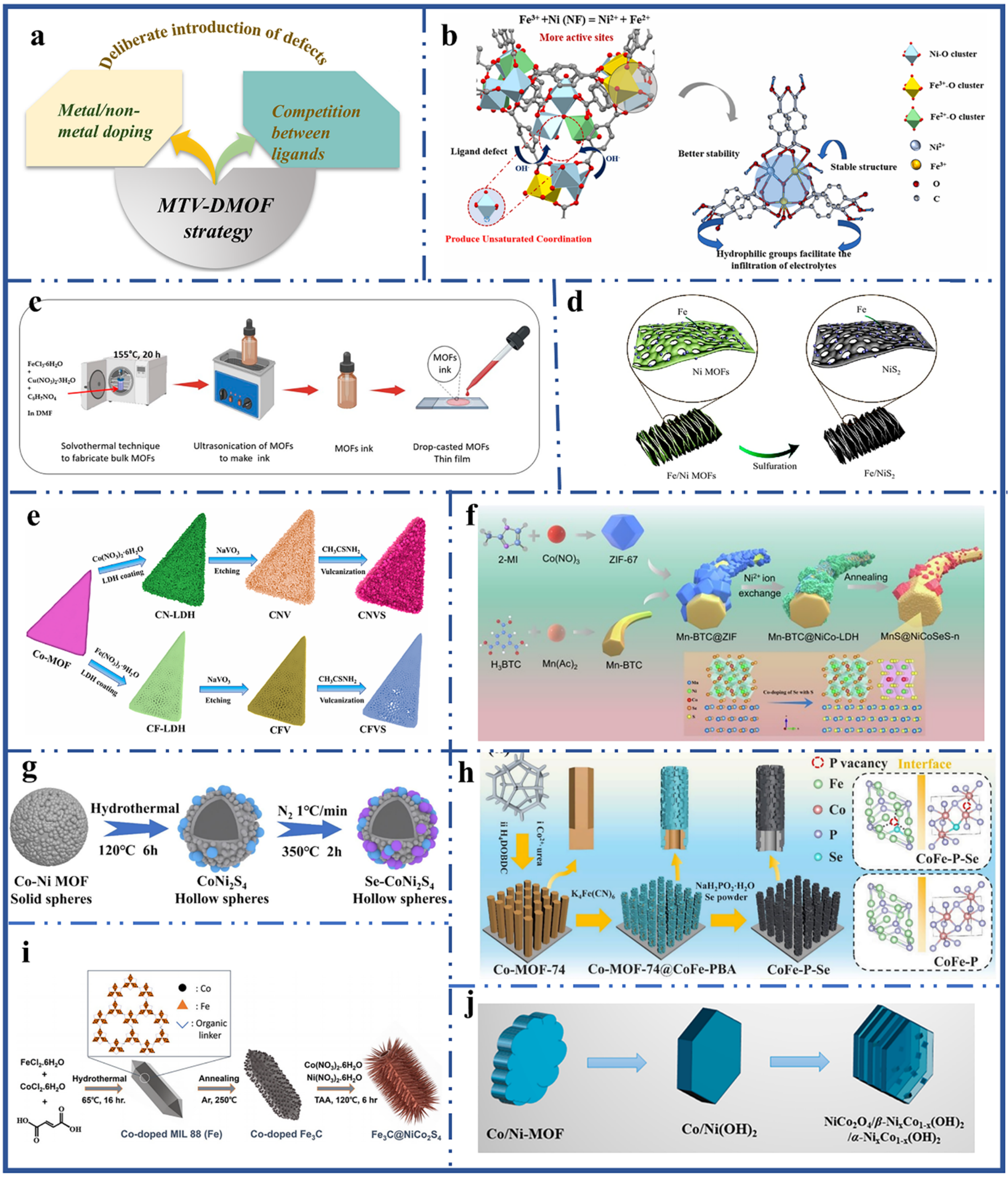

Figure 2. (**a**) MTV-DMOF strategy. (**b**) NiFe-MOF schematic [149]. Copyright 2024, Elsevier. (**c**) Cu@Fe-MOF/NF thin-film electrode preparation [150]. Copyright 2023, MDPI. (**d**) Structure of Fe/NiS2 [151]. Copyright 2023, Elsevier. (**e**) Synthesis of CNVS and CFVS [152]. Copyright 2022, Elsevier. (**f**) MnS@NiCoSeS-1 composites [153]. Copyright 2025, Elsevier. (**g**) Synthesis method for Se-Co CoNi2S4 hollow nanospheres [154]. Copyright 2024, Elsevier. (**h**) Preparation process of CoFe-P-Se [155]. Copyright 2024, American Chemical Society. (**i**) Fabrication process of Fe3C@NiCo2S4 [156]. Copyright 2023, American Chemical Society. (**j**) Method for producing composites [157]. Copyright 2018, American Chemical Society.

Ren and others [153] reported on a MnS@NiCoSeS-1 composite (Figure 2f) synthesized via a MOF-on-MOF oriented selenium-sulfur co-doping technique. This method involves the concurrent doping of Se and S, which is pivotal in defect formation during the material synthesis. Incorporating Se into transition metal sulfides (TMSs) facilitates the creation of additional defects and surface-active sites within the materials, thereby enhancing charge carrier migration, increasing electrical conductivity, and providing more active sites during electrochemical processes. Electrochemical assessments indicated that MnS@NiCoSeS-1 delivered a high specific capacity (up to 901.0 C g^{-1} at 1 A g^{-1}) and exceptional cycling stability (82.6% capacity retention after 10,000 cycles) in a three-electrode system, along with an exceptionally high energy density in a hybrid supercapacitor (HSC) configured in a two-electrode system.

In the synthesis of selenium-doped cobalt-nickel sulfide (Se-$CoNi_2S_4$) hollow nanospheres, as described by Cao et al. [154] and illustrated in Figure 2g, defects primarily associated with selenium doping were observed. The integration of Se into $CoNi_2S_4$ induces significant electronic interactions near the Fermi energy level of the heterojunction, a phenomenon attributed to the considerable ionic radius and low electronegativity of Se. Electrochemical evaluations revealed that the Se-$CoNi_2S_4$ electrode demonstrates an elevated precise capacitance, excellent multiplicity capability, and robust cycling stability, achieving an exact capacitance of 1260 F g^{-1} at 1 A g^{-1} in a three-electrode system.

Cui and others [155] developed electrode materials incorporating Se doping and abundant P vacancies in CoFe-P-Se, as illustrated in Figure 2h. This was achieved using a MOF-on-MOF template approach and a one-pot phosphoselenide method. The generation of defects was primarily attributed to Se doping, which disrupted the original crystallization process of cobalt phosphide (CoP) and iron phosphide (Fe_2P), thereby facilitating the formation of P vacancies. The CoFe-P-Se material demonstrates a specific capacitance of 8.41 F cm^{-2} at a current density of 2 mA cm^{-2}, with a capacity retention rate of 76% after 5000 charge/discharge cycles.

Numerous examples exist of defective MOFs synthesized through metal or non-metal doping, as previously discussed, for application in supercapacitors. For instance, Nwaji and colleagues [156] developed Fe_3C@$NiCo_2S_4$ nanopins to function as electrode materials by utilizing cobalt-doped Fe-MIL-88B as a sacrificial template via a chemical surface transformation method (illustrated in Figure 2i), achieving a unique capacity of 1894.2 F g^{-1} at 1 A g^{-1}. Similarly, Mei et al. [157] employed a bimetallic Co/Ni MOF as a sacrificial template (Figure 2j) to fabricate accordion-like ternary $NiCo_2O_4/\beta\text{-}Ni_xCo_{1-x}(OH)_2/\alpha\text{-}Ni_xCo_{1-x}(OH)_2$ couniquemposites for supercapacitor applications, which achieved a remarkable capacity of 1315 F g^{-1} at 5 A g^{-1}. Liu and coworkers [158] produced an electrode with a considerable specific capacitance of 614 mC cm^{-2} at 1 mA cm^{-2} by uniformly incorporating in-situ P-doped Co_3O_4 nanoparticles into the conductive P-Co_3O_4@PNC. In summary, metal/non-metal doping primarily relies on variations in atomic radii to generate different defects, thereby providing more reaction centers for electrochemical reactions by introducing additional surface-active sites through these defects [159,160]. However, excessive doping may induce lattice strain or disrupt electronic conductivity. Thus, doping concentrations must be optimized to avoid counterproductive effects on electrochemical kinetics. In the MTV-DMOF approach, in addition to metal/non-metal doping, competition among ligands of varying lengths and structures can facilitate defect formation, and unexpected outcomes can be achieved through strategic planning.

3.1.2. Ligand Competition

In the MTV-DMOF approach, in addition to modifying the defect structure of MOFs through metal or non-metal doping, ligand competition emerges as an effective and versatile strategy for defect engineering. Incorporating mixed ligands with distinct geometric differences or coordination capabilities makes it feasible to deliberately induce unsaturated coordination, lattice distortion, or even metal iron deficiency defects within the MOF framework [161,162]. Recently, researchers have successfully developed a variety of defective MOF materials by adjusting the ligand types, ratios, and synthesis conditions, significantly enhancing their charge storage capacity and stability in supercapacitors. For instance, Yue et al. [163] employed a combination of 1,3,5-benzenetricarboxylic acid (H_3BTC) and 4,4′-bis(imidazole-1-yl) biphenyl (BIBP) to synthesize six isostructural MOFs (d^5-d^{10} transition-metal-based MOFs) with a 3D porous structure. As illustrated in Figure 3a, these MOFs were derivatized with three types of carbon morphologies: porous carbon (PC), graphitized carbon (GC), and carbon (C), which were subsequently tested and compared. PC-Zn exhibited the most substantial specific surface area and highest specific capacitance.

Zhang and others [164] utilized a one-step solvothermal synthesis method to fabricate Ni-BTC/IPA, as illustrated in Figure 3b. In this synthesis, H_3BTC and IPA (isophthalic acid) functioned as mixed ligands. However, due to the limited number of carboxylate groups in IPA, it could not form a complete and saturated ligand structure with Ni^{2+} as H_3BTC could. This limitation results in unsaturated coordination at the metal nodes. These defects are instrumental in modulating the electronic structure, pore structure, and active surface sites of MOFs. Electrochemical evaluations indicated that the specific capacitance of Ni-BTC/IPA-3 reached 1209 F g^{-1} at 0.5 A g^{-1}, with a multiplicity performance of 70.8%.

Lin et al. [165] employed the cost-effective benzoic acid (BA) as both a conditioner and ligand in the production of Ni/Co-MOF/NF nanostructured materials, as illustrated in Figure 3c. A significant distinction lies in the difference in the carboxyl group count between BA and the original ligand, terephthalic acid (TPA). During the reaction, BA competes with TPA for metal ions, acting as a non-bridging ligand that partially replaces multi-ligand-bridged TPA. This substitution induces charge repulsion among the MOF layers, resulting in lattice distortion and the formation of defects. These defects increase the number and size of micropores within the MOF, thereby enhancing the surface extent of the electrode. Consequently, the specific capacity of this sample reached 352.3 mAh g^{-1} at a current density of 1 A g^{-1} while maintaining superior cycling steadiness.

Ferhi and others [166] developed an innovative method for integrating polyaniline (PANI) into the nanopores of a defective type MOF-808 (d-MOF-808), as illustrated in Figure 3d. Defective dMOF-808 was prepared by utilizing monocarboxylic acid as a conditioner, with a surfactant self-assembly technique in the reaction. The 60:1 dMOF-808@PANI composite demonstrated the uppermost capacitance of 188 F g^{-1} at 30 mV s^{-1} in a 1 M KOH electrolyte.

Wang and colleagues [167] initially identified a specific defect termed a ligand-induced metal iron deficiency defect. They engineered a porous three-dimensional framework comprising truncated octahedral cage subunits designated as SCNU-Z3. The ligand H_2IPBT, notably, possesses two geometrically analogous end-groups, which achieve more precise coordination upon interaction with Mn^{2+} to form SCNU-Z3. This framework is distinguished by a ligand-induced metal-ion deletion defect, which occurs when the homotopic ligand is replaced with a geometrically similar allosteric ligand.

In addition to the individual applications of metal/non-metal doping or ligand-ligand competition within the MTV-DMOF framework, these methodologies can be integrated into the synthesis of MOFs. For instance, Salehi and coworkers [168] developed a sequence of three-dimensional copper-based MOFs incorporating various metal ions (Co, Zn, and Ni) and different proportions of amine-based functional groups through a solvothermal technique. This was achieved by employing a mixed-metal/ligand strategy, as illustrated in Figure 3e. During the formation of mixed-metal/ligand MOFs, the simultaneous coordination of different metal ions and ligands during crystal growth complicates the formation of a perfectly ordered structure, resulting in defects. Electrochemical testing reveals that the mixed-metal/ligand MOF (Cu–Co (NH_2/50)) demonstrates superior performance, achieving a particular capacitance reaching up to 320.2 F g^{-1} at a current density of 2 A g^{-1}.

It is imperative to ensure that the number of defects introduced through ligand competition is appropriate, as an excessive number of defects can lead to structural collapse, thereby necessitating control over the creation of an 'optimal structure'. For example, Ni/Co-MOF/NF doped with 10% BA maintains a suitable structure, whereas an excess of BA results in structural collapse, and insufficient BA fails to significantly enhance the performance [165]. In conclusion, when implementing the MTV-DMOF strategy, careful selection selects the appropriate doping targets or competing ligands and to precisely determine the specific range of the 'optimal structure'. This approach allows the 'defects' to be utilized effectively for their intended purpose. Only by doing so can the 'defects' be employed appropriately.

3.2. Application of Vacancy Defects in SCs

Vacancy engineering has been employed to optimize materials by introducing specific vacancy defects to modify their properties. This approach is commonly adopted in sectors like energy storage [169–173]. In this paper, the primary focus is on the application of vacancy engineering in SCs.

3.2.1. Oxygen Vacancy

In compounds containing transition metals, oxygen vacancies significantly enhance their electrochemical properties. This improvement is attributed to the vacancies' capacity to augment OH^- absorption and electronic conductivity, thereby increasing the Faraday reaction activity [174]. Numerous examples have demonstrated the utilization of oxygen vacancies to enhance the performance of SCs. For instance, Zhu et al. [175] developed double-defect-modulated MOF-derived P-Co_3O_4@NC@O_v-NiMnLDH heterostructures through P doping and the creation of oxygen vacancies. In this context, oxygen vacancies were generated via a wet chemical reduction method, wherein the prepared electrode was immersed in a $NaBH_4$ solution for a specified duration. This process exploits the reducing properties of $NaBH_4$ to interact with surface oxygen atoms onto the composite, causing some to detach from the crystal lattice and form oxygen vacancy defects. Electrochemical evaluations indicated that this double-defect modulated electrode outperforms both single-defect and defect-free electrodes, achieving a specific capacity of up to 285.56 mA h g^{-1} at 1 A g^{-1}.

Wei and others [176] have developed a composite material by integrating NiCo-LDH with MXene, which is derived from MOF. MXene surfaces contain abundant functional groups with high electronegativity, such as –F, –OH, and –O. These groups enhance the attraction of the hydroxyl groups to the metal ions during MXene etching. When combined with NiCo-LDH, the hydroxyl groups on the MXene surface attracted Ni and Co ions with unsaturated coordination from NiCo-LDH, displacing some ions from their original lattice sites and forming oxygen vacancies. Theoretical calculations suggest that these oxygen vacancies facilitate charge carrier migration, enabling the MXene@NiCoLDH electrode to achieve a particular capability of 163.25 mA h g^{-1} at 1 A g^{-1}. Furthermore, the energy density of the resulting supercapacitor is 46.10 Wh kg^{-1} at a power density of 1170.38 W kg^{-1}.

Chettiannan et al. [177] successfully synthesized $NiO/Co_3O_4/NiCo_2O_4$ composites by meticulously controlling the mass ratio between Ni-MOF and Co-MOF. Notably, the NC41 composite, produced with a 4:1 ratio, demonstrates high crystallinity (as depicted in Figure 3f), a distinctive microstructure, a substantial specific surface area, and numerous surface oxygen defects, culminating in a certain volume of 1108.9 C g^{-1}.

Guo and colleagues [178] synthesized ZnCoO/C composites by varying the Zn/Co ratio. During the synthesis process, the Zn atoms progressively replaced the Co atoms in Co_3O_4, forming $ZnCo_2O_4$. As the proportion of Zn atoms increased, oxygen vacancies were introduced into the $ZnCo_2O_4$ crystals, as illustrated in Figure 3g. The ZnCoO/C-2 electrode demonstrated a certain volume of 356.3 F g^{-1} at 1 A g^{-1}, with exceeding 77% capacitance fade resistance after 10,000 cycles, indicating excellent cycling stability.

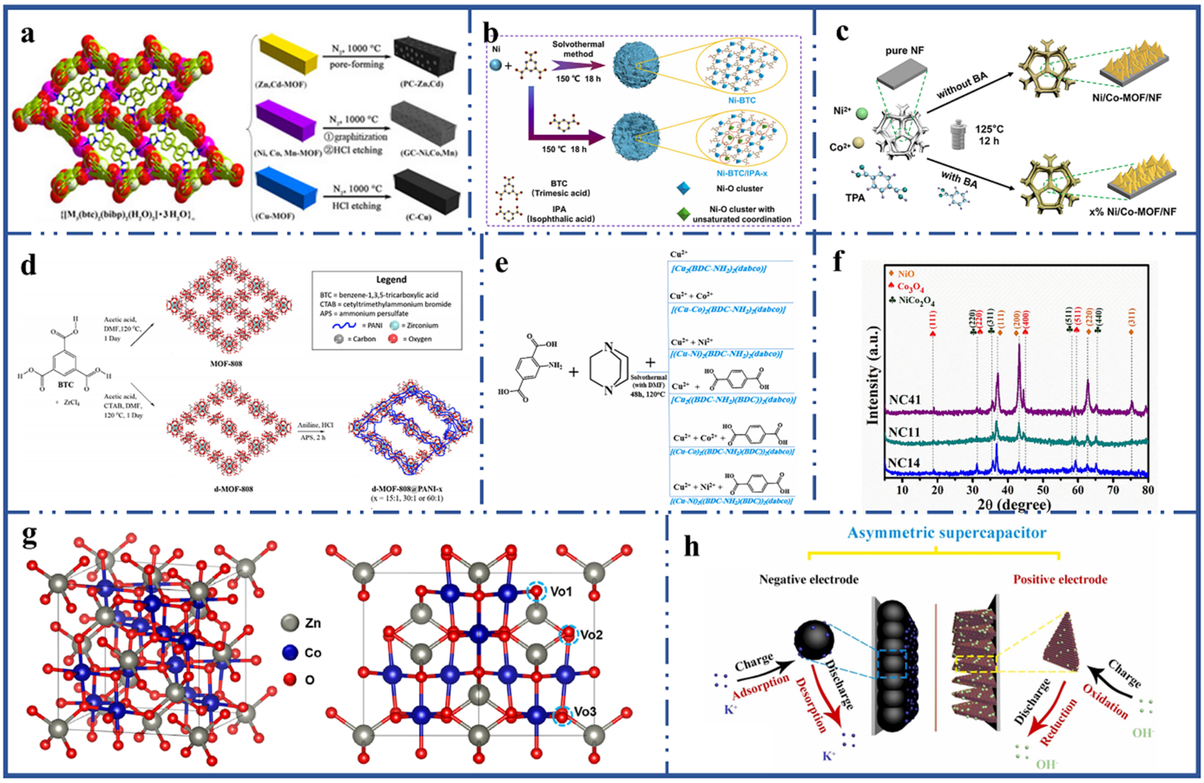

Figure 3. (**a**) A collection of isostructural MOFs and their resulting carbon formations [163]. Copyright 2018, John Wiley and Sons. (**b**) Method for creating Ni-BTC/IPA [164]. Copyright 2024, Elsevier. (**c**) Process for synthesizing Ni/Co-MOF/NF [165]. Copyright 2024, American Chemical Society. (**d**) Procedure for developing dMOF-808@PANI [166]. Copyright 2022, American Chemical Society. (**e**) Detailed method of the mixed metal/ligand approach [168]. Copyright 2022, Elsevier. (**f**) Various proportions of $NiO/Co_3O_4/NiCo_2O_4$ as determined by XRD [177]. Copyright 2024, Elsevier. (**g**) Left: configuration of $ZnCo_2O_4$; Right: oxygen vacancies within $ZnCo_2O_4$ crystals [178]. Copyright 2024, Elsevier. (**h**) Diagram of Zn/Co-S@CeO_2//AC [179]. Copyright 2023, Elsevier.

Xu and coworkers [179] developed a self-supporting Zn/Co-S@CeO_2 heterostructured nanosheet array electrode by incorporating CeO_2 nanoparticles onto the surface of Zn/Co-S derived from a MOF. The fabrication of this electrode involved three stages: the creation of Zn/Co-MOF nanoarrays, sulfurization to form Zn/Co-S, and the addition of CeO_2. The defects primarily pertain to oxygen vacancies in CeO_2, which are significantly influenced by the metastable characteristics of CeO_2 and the preparation method. As illustrated in Figure 3h, the asymmetric supercapacitor (ASC) fabricated with the as-obtained composite and negative AC (activated carbon) exhibits an elevated energy-density value of 42.4 Wh kg^{-1} and outstanding cycling durability. It maintains 91.1% of its capacitance even after 8000 charge-discharge cycles.

Chen et al. [180] successfully synthesized defect-rich NiMo-LDH/MOF-1 nanoflower heterostructures via a two-step solvothermal method (as depicted in Figure 4a), employing Ni-MOF as a template and incorporating oxygen vacancies. NiMo-LDH/MOF-1 demonstrated a specific capacitance of 2516 F g^{-1} at 1 A g^{-1}, indicating an exceptional multiplicity performance. The fabricated NiMo-LDH/MOF-1//AC ASC achieved an energy density of 58.6 Wh kg^{-1} at a power density of 800 W kg^{-1}, retained 83.8% of its capacitance after 9000 cycles, and exhibited a Coulombic efficiency of 100%.

Mofokeng and coworkers [181] synthesized Ni-MOF utilizing a microwave-assisted solvothermal method and subsequently produced Ni/MOFDC and AT-Ni/MOFDC (as illustrated in Figure 4b) through processes of carbonization and acid treatment. Acid treatment, also known as the etching process, induces the formation of numerous oxygen vacancies in AT-Ni/MOFDC, thereby enhancing its electrochemical performance. Compared to Ni/MOFDC, which possesses a specific capacity of 92 mAh g^{-1}, AT-Ni/MOFDC demonstrates a reduced series resistance and an increased specific capacity of 199 mAh g^{-1}.

Yang et al. [182] synthesized two distinct morphologies of Bi_2O_3 powders: c-Bi_2O_3, produced via calcination, and h-Bi_2O_3, developed through a two-step hydrothermal process, for application in supercapacitor electrodes. During the hydrothermal synthesis of h-Bi_2O_3, an elevated concentration of OH^- ions facilitated the formation of additional oxygen vacancies. The increased partial pseudo capacitance and conductivity, attributed to the higher prevalence of $V_{Bi}''V_O''V_{Bi}''$ defects (as depicted in Figure 4c), enabled h-Bi_2O_3 to achieve a particular capability of up to 1043 F g^{-1} at 1 A g^{-1}, with a capacitance retention of up to 93% after 2000 cycles at 50 A g^{-1}.

Wei and others [183] utilized a bottom-up methodology to synthesize ZIF-67 nanosheets, which were subsequently converted into Co_3O_4 ultrathin nanonets through in situ heat treatment, as illustrated in Figure 4d. Throughout the annealing procedure, the atomic proportion of Co^{2+}/Co^{3+} and the appearance of oxygen vacancies were fine-tuned to uphold the electrical neutrality of the entire framework, thereby bringing about the emergence of oxygen defects.

Numerous studies have shown that oxygen vacancies can be exploited to boost the performance of SCs. For example, Wang et al. [184] developed CoAlLDH with oxygen vacancies through $NaBH_4$ treatment, achieving a specific capacity of 799.2 F g^{-1}, which surpasses that of the original CoAlLDH. Wei and others [185] employed MXene as a substrate to cultivate NiCo-MOF (depicted in Figure 4e). The hydroxyl sites on MXene facilitate the adsorption of metal ions through weak coordination, giving rise to oxygen deficiencies and an increased electron transfer rate. Li and coworkers [186] created NiMnMg-LDH@3DG using 3D graphene foam as a template (illustrated in Figure 4f), which resulted in an impressive specific capacity and commendable cycling stability. Moreover, oxygen vacancies boost the electrode’s affinity for OH^-, enhancing electrolyte ion mobility. Tang et al. [187] produced NiMn LDH with oxygen vacancies (referred to as O_v-LDH, with the preparation process shown in Figure 4g) through mild H_2O_2 treatment, achieving a peak specific capacity of 1183 C g^{-1}, significantly better than untreated NiMn LDH. Chen and coworkers [188] synthesized NiCo-LDH via in-situ growth and incorporated oxygen vacancies to modify the electronic structure (the material with oxygen vacancies was named O_vIS-LDH, and the preparation process is depicted in Figure 4h), which reduced charge transfer resistance and achieved a remarkable capacity of 1111 C g^{-1} at 1 A g^{-1}. In conclusion, the incorporation of oxygen vacancies can modify the electronic configuration of the material, thereby increasing electrical conductivity, the number of active surface sites, and improving the degree of structural stability [189,190], making it an effective strategy to exploit defects for improving SC performance. Besides oxygen vacancies, other types of vacancies, such as sulfur and phosphorus vacancies, can also enhance the SC performance to a certain degree.

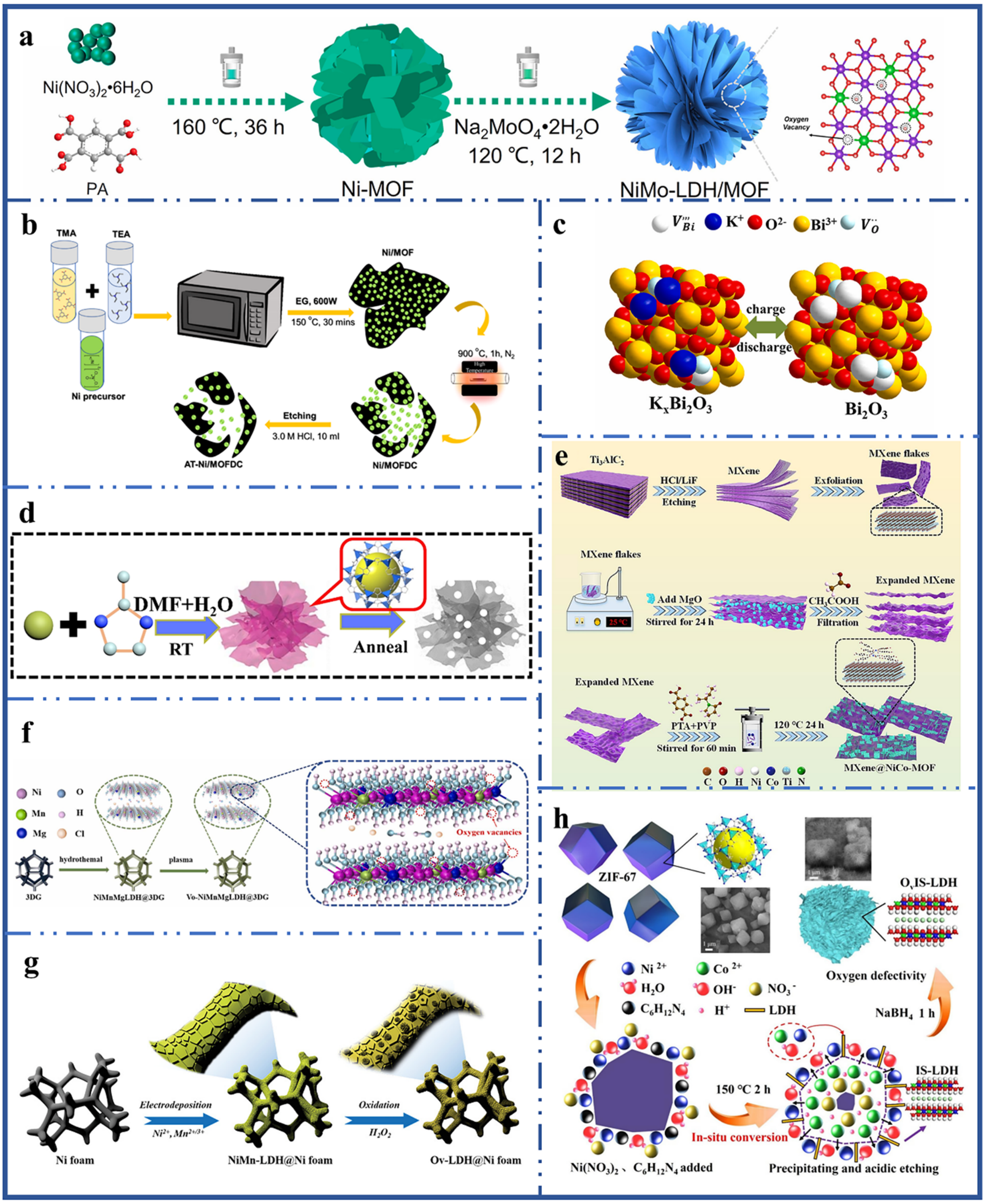

Figure 4. (**a**) NiMo-LDH/MOF-1 preparation process [180]. Copyright 2025, Elsevier. (**b**) Ni/MOFDC and AT-Ni/MOFDC preparation [181]. Copyright 2020, American Chemical Society. (**c**) Diagram illustrating the pseudo-capacitance origin of h-Bi_2O_3 [182]. Copyright 2021, Elsevier. (**d**) M-Co_3O_4 ultrathin nanonets preparation [183]. Copyright 2018, American Chemical Society. (**e**) MXene@NiCo-MOF preparation [185]. Copyright 2024, Elsevier. (**f**) Diagram showing the preparation of NiMnMg-LDH@3DG [186]. Copyright 2024, Elsevier. (**g**) O_v-LDH preparation [187]. Copyright 2020, John Wiley and Sons. (**h**) O_vIS-LDH preparation [188]. Copyright 2024, Elsevier.

3.2.2. Sulphur Vacancy

Research has indicated that introducing sulfur vacancies into electrode materials can enhance their electrical conductivity and electrochemical characteristics [191]. Concurrently, an embedded electric field arises owing to the uneven redistribution of charges, which facilitates the migration of ions and electrons [192]. For instance, Wang et al. [193] described a straightforward and efficient method (Figure 5a) for creating phosphorus-doped CoS (P-CoS_{1-x}) nanosheets with sulfur defects, which were deposited on carbon nanotube thin films (CNTs) through a one-step hydrothermal process involving sulfurization, phosphorylation, and reduction. In this process, phosphorus doping and sulfur defects contributed to improvements in the oxygen evolution reaction (OER) and electrochemical properties of CoS. The resulting flexible asymmetric supercapacitor (P-CoS1−x//CoS@PPy) also demonstrated an elevated energy density of 0.18 m Wh cm^{-2} and excellent bending stability.

Nwaji and others [194] successfully synthesized cubic cobalt-based MOFs with Fe additives and subsequently transformed them into core-shell hollow-tubes with S vacancies through a straightforward method at room temperature. The presence of numerous S vacancies, a porous architecture, multi-metallic species, and Fe component in the Fe-Co_2S_3@$CoMo_2S_4$ composition results in a unique nanostructure that facilitates Faraday redox reactions, thereby enhancing charge transfer pathways and significantly reducing the opposition of the material. This causes a specific capacitance of 980.5 F g^{-1} at a current intensity of 1 A g^{-1}, along with excellent rate performance and cycling steadiness.

Chen and colleagues [195] developed r-$NiCo_2S_4$ hollow microsphere electrode material characterized by sulfur vacancies, as depicted in Figure 5b, through a procedure encompassing ligand substitution and chemical deoxidization. The generation of sulfur vacancies was accomplished via a chemical reduction method, specifically a $NaBH_4$ treatment. During this procedure, some Co^{3+} were partially reduced to Co^{2+}, while the concentration of Ni^{2+} increased, facilitating electron transfer and forming sulfur vacancies. In a three-electrode system, r-$NiCo_2S_4$ demonstrated a high specific capacitance of up to 1406.4 F g^{-1} (1 A g^{-1}), with a multiplicity performance of 90.03% and a capacitance maintenance of 87.5% after 10,000 cycles.

In addition to the previously mentioned examples, numerous other applications exist for S defects in SCs. For instance, Wang et al. [192] generated S vacancies in $NiCo_2S_4$ through plasma introduction, yielding a capacity significantly greater than that of $NiCo_2S_4$ without S vacancies. Huang and others [196] produced NiS@C hollow structures with S vacancies (Figure 5c), achieving a high reversible specific capacity of 1728 F g^{-1} at 1 A g^{-1}. In summary, S vacancies can enhance material conductivity, increase active sites, and promote charge redistribution to generate an inherent electric field, thereby improving electron/ion diffusion during reactions [197]. The strategic utilization of S vacancies in supercapacitors can facilitate the targeted preparation of high-performance materials.

3.3. Application of Other Defect Methods in SCs

In addition to conventional methodologies, such as MTV-DMOFs and vacancy engineering, emerging techniques, including etching, laser-assisted processing, and pyrolysis-induced defects, present novel opportunities for defect modulation in MOFs. These innovative approaches have significantly enhanced the specific capacity, energy density, and cycling stability of SCs by precisely modifying the pore structure, surface chemistry, and electronic properties of the materials. The most recent advancements in defect engineering strategies are delineated below.

3.3.1. Etching Techniques

Etching is a technique employed to isolate a target defective material through chemical or physical methods [198–200]. This process is classified into chemical, electrolytic, and dry etching, with chemical etching being commonly utilized for inducing defects in MOFs. Chemical etching includes approaches such as acid, alkaline, and oxidative etching. By selecting an appropriate etchant and modifying the etching conditions, specific components within MOF materials can be selectively removed or their surface structures modified, thereby enabling accurate control over the pore volume, morphology, and surface characteristics of MOFs [201,202]. This discussion focuses on the predominant methods of acid and alkaline etching.

Acid etching is a rapid process typically conducted using acidic solutions, such as sulfuric and hydrochloric acids [203,204]. For example, Gao and others [205] introduced defects in graded porous Zr-MOFs (HP-UiO-66) by removing acid-sensitive ZnMOFs through acid treatment involving immersion in a hydrochloric acid solution with a pH of 1.0 (Figure 5d). This acid etching altered the crystalline framework of the material, yielding a particular capacitance of 849 F g^{-1} at a current density of 0.2 A g^{-1} for HP-UiO-66. This value far surpasses the 101.5 F g^{-1} of pristine UiO-66. The improved performance can be ascribed to the hierarchical porous architecture, large specific surface area and pore volume, and surface irregularities. Xiong and colleagues [206] developed Ni/NiO/CoO-CW-x electrode material by etching it with HNO_3 (Figure 5e). The solid-state supercapacitor based on this electrode exhibited an energy density of 0.67 mWh cm^{-2} (8.38 mWh cm^{-3}) and demonstrated excellent cycling stability, retaining 96.21% of its capacitance after 10,000 cycles.

Alkaline etching, recognized for its slower rate and enhanced safety, typically employs various solutions, such as sodium hydroxide and copper hydroxide [207,208]. Lu and others [209] synthesized mesoporous cobalt carbonate hydroxide nanosheets by utilizing NaOH as an etchant to remove Al^{3+} from CoAl-LDH, achieving a maximum capacitance of 1075 F g^{-1} at a current density of 5 mA cm^{-2}. Yue et al. [210] fabricated a ZnCoNiP-D metal phosphide electrode (Figure 5f) using a bimetallic organic framework, Zn/Co-MOF, as a self-sacrificing precursor. This procedure involved a hydrothermal reaction, alkaline etching with NaOH, and low-temperature phosphitylation, resulting in a capacity of 770.4 C g^{-1} at 1 A g^{-1} and a capacity maintenance of 81.8% after 5000 charge/discharge cycles.

In addition to the conventional use of specific acid and alkali etchants for etching, this process can be achieved under certain conditions. For example, Hassan et al. [211] developed supercapacitor-type electrodes, N-MXene, by self-assembling Cu-BTC MOF on N-$Ti_3C_2T_x$ MXene and conducting in situ etching, which resulted in a high specific capacity.

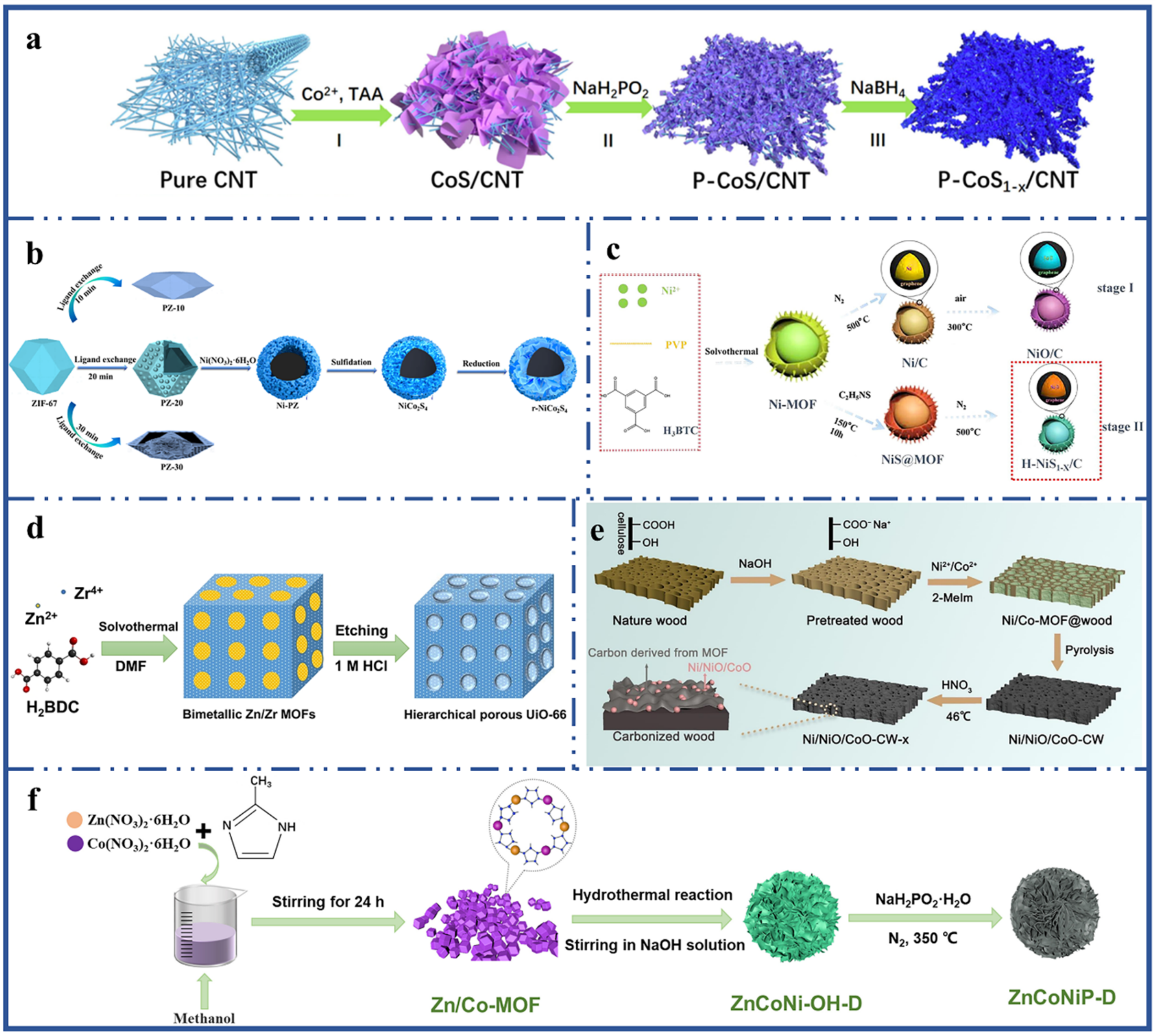

Figure 5. (**a**) Process for preparing P-CoS_{1-x} nanosheets [193]. Copyright 2022, Elsevier. (**b**) Method for synthesizing r-$NiCo_2S_4$ [195]. Copyright 2022, Elsevier. (**c**) Procedure for creating NiS@C hollow structures [196]. Copyright 2021, Elsevier. (**d**) Methodology for producing HP-UiO-66 [205]. Copyright 2017, American Chemical Society. (**e**) Process for fabricating Ni/NiO/CoO-CW-x [206]. Copyright 2025, Elsevier. (**f**) Preparation technique for ZnCoNiP-D [210]. Copyright 2023, Elsevier.

3.3.2. Other Defect Methods in SCs

As advancements in science and technology continue, a growing array of innovative defect engineering methods is being explored. Beyond conventional approaches, novel techniques such as pyrolysis, laser treatment, template transformation, and composite design have significantly enhanced the charge storage capacity and cycling stability of supercapacitors. This enhancement is achieved through the modification of the pore structure, surface defects, and component synergies of the materials. These approaches boost the specific surface area and electrical conductance of electrode materials by inserting gradient pores, metal-excess imperfections, or non-uniform structures, thus presenting multiple routes for developing high-performance energy storage apparatuses. Each of these methods is elaborated upon in the following sections.

The pyrolysis process facilitates the removal of specific ligands, resulting in the formation of pores of diverse sizes and the establishment of a hierarchical pore structure. This structural modification can enhance the specific surface area of the material, thereby providing additional active sites [212,213]. In the study conducted by Chen et al. [214], the synthesis of N-doped bimetallic sulfide hollow spheres (HN_2CMS), as illustrated in Figure 6a, was achieved through the pyrolysis of organic components, leading to the formation of a hollow shell structure. The HN_2CMS electrode demonstrated a definite capacitance of 938.1 C g^{-1} at 1 A g^{-1} in a 3M KOH electrolyte, maintaining a capacitance retention rate of 85.0% after 5000 cycles, with low resistance and excellent cycling stability.

Laser-assisted processing is a technological method that harnesses laser energy to accomplish specific objectives in material preparation or alteration and is now also employed in defect creation. For instance, Aashi and others [215] generated defects in CuZn–BTC MOF materials through laser irradiation (Figure 6b). In this scenario, the laser irradiation energy influences the structure of the material, leading to an increased electrode surface area and improved specific capacitance. Among the various laser power levels (2 W, 5 W, 7 W, 10 W, 12 W), the optimized CuZn-MOF-P7 (laser power is 7 W) exhibits the highest performance, achieving a particular capacitance of 3.7 F cm^{-2} at a current density of 1 mA cm^{-2} and maintaining 97% of its capacitance after 16,000 cycles.

Cao and colleagues [216] developed highly oriented octagonal nanohybrid materials of cobalt-doped Cu-MOF/$Cu_{2+1}O$ through an in situ reverse transformation method, utilizing vertically aligned $Cu(OH)_2$ nanorod arrays as both templates and precursors. During this transformation, the chemical environment of elemental copper changes, causing excessive amount of copper within the Cu_2O lattice, resulting in the formation of $Cu_{2+1}O$ with unique properties. The optimized (0.1Co/Cu-MOF/$Cu_{2+1}O$) electrodes demonstrate a significant areal capacity of 1.548 F cm^{-2} (equivalent to 518.58 F g^{-1}) and exhibit excellent cycling stability, retaining 97.26% of their capacity after 5000 cycles.

Zheng et al. [217] successfully synthesized $Cu_{2+1}O$@Cu-MOF cluster arrays in situ using a gas-phase technique. In this process, the $Cu(OH)_2$ nanorods on Cu foam is used as both precursors and templates, and were exposed to sublimated terephthalic acid ligand gases (Figure 6c). During the thermal transformation from $Cu(OH)_2$ to $Cu_{2+1}O$, changes in the crystal structure occur, resulting in excess metal defects. The resultant material exhibits a specific capacitance of up to 2.5 F cm^{-2} within a three-electrode system.

Gao and coworkers [218] successfully synthesized MnS_2/MnSe@HCMs, which are sulfur and selenium co-doped hollow porous carbon microsphere-encapsulated MnS_2/$MnSe_2$ heterostructure nanoparticles, via a one-step sulphation/salination process utilizing Mn-MOF as the precursor material (as illustrated in Figure 6d). This material demonstrated an outstanding specific capacity of 1340.2 C g^{-1} under a current density of 10 A g^{-1}, maintaining 85.8% of its capacity following 10,000 cycles.

Wu et al. [219] synthesized MIL101(Fe) derivatives utilizing carbonization and continuous carbonization/oxidation technique, as illustrated in Figure 6e. In this methodology, a lower carbonization temperature leads to a less-ordered carbon structure and the formation of additional defects. The MIL101(Fe)-C electrode, carbonized at 800 °C, exhibited the highest specific capacitance of 95.7 F g^{-1} at a scan rate of 20 mV s^{-1}. This superior performance is attributed to its rough surface, hollow structure, and optimal defect-to-graphitization ratio.

In addition to the distinctive treatment of materials, the performance of SCs may be improved by integrating them with specific specialized materials. During the fabrication of these composites, certain defects may be introduced to immobilize specific metal ions. Su and others [220] developed an aerogel with a uniform microporous structure (PEDOT:PSS) through directional freezing. UiO-66 was cultivated within this structure, and Mn sites were immobilized to form a Mn-UiO-66/PEDOT:PSS composite aerogel, which was subsequently employed in SCs (the preparation process is illustrated in Figure 6f).

Li et al. [221] successfully engineered a porous, nest-like structure on activated carbon cloth (ACC) for the positive electrode, while concurrently employing nitrogen-doped ACC (NAC) for the negative electrode, as depicted in Figure 6g. The ASC fabricated from these materials achieved an energy density of 1.09 mWh cm^{-2} and a power density of 17 mW cm^{-2} within a voltage range of 0 to 1.65 V. It exhibited remarkable cycling stability, maintaining 89.43% of its capacitance after 7000 cycles.

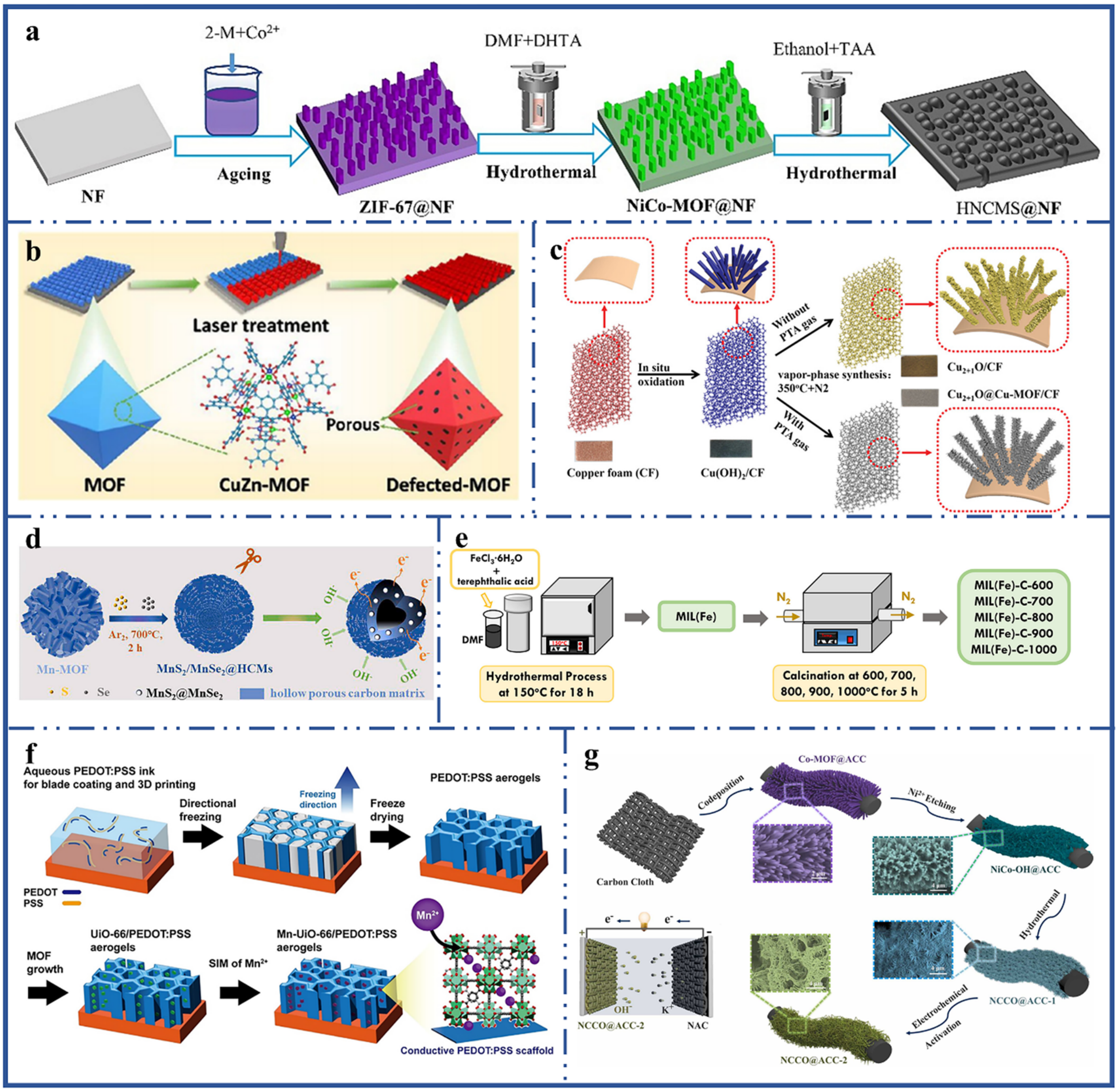

Figure 6. (**a**) The method for preparing HN_2CMS [214]. Copyright 2023, Elsevier. (**b**) A schematic representation of CuZnMOF subjected to lasers with varying power levels [215]. Copyright 2024, American Chemical Society. (**c**) The process for creating $Cu_{2+1}O$@Cu-MOF [217]. Copyright 2021, John Wiley and Sons. (**d**) The method for synthesizing MnS_2/MnSe@HCMs [218]. Copyright 2024, Elsevier. (**e**) The procedure for producing MIL101(Fe) derivatives [219]. Copyright 2022, Elsevier. (**f**) The preparation of Mn-UiO-66/PEDOT:PSS [220]. Copyright 2025, American Chemical Society. (**g**) The process for forming positive and negative electrodes on activated carbon cloth (ACC) [221]. Copyright 2024, Elsevier.

Defect engineering is a crucial method for boosting the performance of MOF-based supercapacitors. Using techniques such as acid/alkali etching, oxidative etching, laser processing, pyrolytic conversion, and composite strategies, researchers can precisely introduce graded pores, metal-excess defects, or heterostructures. These modifications enhance the ion diffusion kinetics, electron conduction, and exposure of the active sites. A more profound understanding of the structure, particularly concerning defect modulation, leads to improved performance of SCs. To systematically summarize the performance and mechanisms of defect-engineered MOFs in supercapacitors, key cases from recent studies are compiled in Table 1, which compares specific capacitance, cycling stability, and defect-induced enhancements across different strategies. This synthesis highlights the synergistic effects between structural defects and electrochemical performance, providing a roadmap for future material design.

Table 1. Summary of defect engineering applications in MOF-based supercapacitors (partial).

Defect Type	Material/Structure	Key Performance Metrics	Mechanism of Enhancement	Ref.
Metal Doping	NiFe-MOF nanosheets	Specific area capacitance: 15.6 F cm^{-2} at 2 mA cm^{-2} Capacitance retention: 86.3% after 5000 cycles	Fe^{3+}/Fe^{2+} doping induces lattice stress, forming thinner nanosheets with increased active sites	[149]
	Cu@Fe-MOF/NF thin film	Specific capacitance: 420.54 F g^{-1} at 3 A g^{-1}	Cu doping modifies electron distribution and creates coordinative defects	[150]
	Fe-doped NiS_2 ($Fe_{0.01}NiS_2$)	Specific capacitance: 1965.9 F g^{-1} at 0.5 A g^{-1}	Fe doping introduces lattice stress and defects due to atomic radius mismatch	[151]
Non-metal Doping (Se/P)	Se-$CoNi_2S_4$ hollow nanospheres	Specific capacitance: 1260 F g^{-1} at 1 A g^{-1}	Se doping induces electronic interactions near Fermi level and creates sulfur vacancies	[154]
	CoFe-P-Se (Se-doped, P vacancies)	Specific capacitance: 8.41 F cm^{-2} at 2 mA cm^{-2} Retention: 76% after 5000 cycles	Se doping disrupts crystallization, forming P vacancies and enhancing charge transport	[155]
Ligand Competition	Ni-BTC/IPA (H_3BTC + IPA ligands)	Specific capacitance: 1209 F g^{-1} at 0.5 A g^{-1} Rate performance: 70.8%	IPA's limited carboxylate groups cause unsaturated metal coordination and improved porosity	[164]
	Ni/Co-MOF/NF (BA-doped)	Specific capacity: 352.3 mAh g^{-1} at 1 A g^{-1}	BA competes with TPA, inducing lattice distortion and increasing micropore density	[165]
Oxygen Vacancies	P-Co_3O_4@NC@O_v-NiMnLDH heterostructure	Specific capacity: 285.56 mAh g^{-1} at 1 A g^{-1} (superior to single-defect counterparts)	$NaBH_4$ reduction creates oxygen vacancies, enhancing OH^- adsorption and conductivity	[175]
	MXene@NiCoLDH composite	Specific capacity: 163.25 mAh g^{-1} at 1 A g^{-1} Energy density: 46.10 Wh kg^{-1}	MXene's hydroxyl groups induce oxygen vacancies via metal ion displacement	[176]
	NiO/Co_3O_4/$NiCo_2O_4$ (NC41 composite)	Specific volume: 1108.9 C g^{-1}	Controlled mass ratio induces surface oxygen defects and high crystallinity	[177]
Sulfur Vacancies	r-$NiCo_2S_4$ hollow microspheres	Specific capacitance: 1406.4 F g^{-1} at 1 A g^{-1} Retention: 87.5% after 10,000 cycles	$NaBH_4$ treatment reduces Co^{3+} to Co^{2+}, creating sulfur vacancies and enhancing electron transfer	[195]
Etching (Acid/Alkali)	HP-UiO-66 (HCl-etched Zr-MOF)	Specific capacitance: 849 F g^{-1} at 0.2 A g^{-1} (8× higher than pristine UiO-66)	Acid etching removes ZnMOF, creating hierarchical pores and surface irregularities	[205]
	ZnCoNiP-D (NaOH-etched Zn/Co-MOF)	Specific capacity: 770.4 C g^{-1} at 1 A g^{-1} Retention: 81.8% after 5000 cycles	Alkaline etching removes Al^{3+}, forming mesoporous metal phosphides with defect-rich surfaces	[210]
Pyrolysis/Laser Treatment	HN_2CMS	Specific capacitance: 938.1 C g^{-1} at 1 A g^{-1} Retention: 85% after 5000 cycles	Pyrolysis decomposes MOF ligands, creating hollow shells and gradient pores for fast ion transport	[214]
	CuZn-MOF-P7 (laser-irradiated)	Specific capacitance: 3.7 F cm^{-2} at 1 mA cm^{-1} Retention: 97% after 16,000 cycles	Laser energy disrupts MOF lattice, increasing surface area and defect density	[215]

4. Conclusions

This study investigates the advancements in defect engineering within metal-organic framework (MOF) materials to enhance the performance of supercapacitors (SCs). MOFs are regarded as an outstanding option for SC electrode materials due to their extensive specific surface area, customizable pore architecture, and abundant active sites. By employing defect engineering techniques, such as metal/non-metal doping, ligand competition, and vacancy defects, the electronic structure, ion transport kinetics, and surface-active sites of MOFs can be optimized to significantly improve the energy density, power density, and cycling stability of SCs. The use of a multivariate defect MOF (MTV-DMOF) and vacancy engineering, including oxygen and sulfur vacancies, offers innovative approaches for boosting SC performance. Furthermore, new methods, such as etching, laser-assisted processing, and pyrolysis-induced defects, have introduced novel possibilities for defect modulation in MOFs. In addition, although not covered in detail in this review, nitrogen and carbon vacancies have also been shown to potentially influence the electrochemical performance of MOF-based materials, according to relevant studies. Future research could focus on exploring the effects of these vacancies, which might provide new insights into improving the performance of supercapacitors.

Future research should explore defect-electrochemistry relationships and address inherent limitations of defect engineering. For instance, excessive defects may induce structural fragility (e.g., ligand competition-induced framework collapse) or electronic disorder (e.g., sulfur vacancy-mediated charge trapping). Developing in situ characterization tools to monitor defect dynamics during operation and establishing defect tolerance thresholds will be crucial for designing robust MOF-based energy storage systems. Additionally, integrating in situ characterization with computational simulations to elucidate the dynamic changes in defects will establish a novel framework for designing high-performance MOF-based energy storage materials.

Beyond fundamental studies, practical applications demand scalable synthesis methods. Recent advances in modular synthesis, such as flow chemistry and 3D printing of MOF composites, show promise for industrial-scale production of defect-engineered MOFs. Moreover, coupling defect engineering with hybrid architectures (e.g., MOF/graphene heterostructures or MXene@MOF hybrids) could further enhance charge transfer kinetics and mechanical stability, addressing challenges in flexible and wearable energy storage devices. For instance, lightweight MOF-based micro-supercapacitors integrated into smart textiles or IoT sensors could revolutionize portable electronics. Environmentally sustainable strategies, such as bio-MOFs derived from natural ligands or recyclable MOF templates, should be prioritized to align with global carbon neutrality goals. Finally, exploring multi-defect synergy (e.g., oxygen vacancies coupled with sulfur defects) and their interfacial interactions with electrolytes may unlock unprecedented energy densities (>50 Wh kg^{-1}) while maintaining ultrahigh power densities (>10 kW kg^{-1}), bridging the gap between batteries and conventional capacitors. These efforts will accelerate the transition from laboratory-scale breakthroughs to commercial energy storage solutions.

Author Contributions

K.W.: conceptualization, methodology, reviewing and editing, supervision; R.F.: data curation, writing—original draft preparation; L.W.: visualization, investigation; X.Y.: validation, investigation; C.L.: software, writing—reviewing and editing; M.O.: investigation; H.W.: validation, software; R.X.: writing—reviewing and editing. All authors have read and agreed to the published version of the manuscript.

Funding

This work was supported by the National Natural Science Foundation of China (22279061), the Fundamental Research Funds of Central Universities (KYCXJC2023004, KYGD202107), and the Natural Science Foundation of Jiangsu Province (BK20180514).

Institutional Review Board Statement

Not applicable.

Informed Consent Statement

Not applicable.

Data Availability Statement

We declare that we have no financial and personal relationship with other people or organizations that can inappropriately influence our work, and there is no professional or other personal interest of any nature or kind in any data, service, product and/or company that could be construed as influencing the position presented in the manuscript entitled.

Acknowledgments

The authors gratefully acknowledge Cheng Zhang for his technical guidance in plotting and composing.

Conflicts of Interest

The authors declare no conflict of interest.

References

1. Abazari, R.; Sanati, S.; Fan, W.K.; et al. Design and engineering of MOF/LDH hybrid nanocomposites and LDHs derived from MOF templates for electrochemical energy conversion/storage and environmental remediation: Mechanism and future perspectives. *Coord. Chem. Rev.* **2025**, *523*, 216256. https://doi.org/10.1016/j.ccr.2024.216256.
2. Liu, J.; Fu, G.; Liao, Y.; et al. Electrochemical conversion of small organic molecules to value-added chemicals and hydrogen/electricity without CO_2 emission: Electrocatalysts, devices and mechanisms. *eScience* **2025**, *5*, 100267. https://doi.org/10.1016/j.esci.2024.100267.
3. Chen, L.; Yu, C.; Dong, J.; et al. Seawater electrolysis for fuels and chemicals production: Fundamentals, achievements, and perspectives. *Chem. Soc. Rev.* **2024**, *53*, 7455–7488. https://doi.org/10.1039/D3CS00822C.
4. Bi, H.; Liu, J.; Wang, L.; et al. Selective contact self-assembled molecules for high-performance perovskite solar cells. *eScience* **2025**, *5*, 100329. https://doi.org/10.1016/j.esci.2024.100329.
5. Su, Y.; Yuan, G.; Hu, J.; et al. Thiosalicylic-Acid-Mediated Coordination Structure of Nickel Center via Thermodynamic Modulation for Aqueous Ni–Zn Batteries. *Adv. Mater.* **2024**, *36*, 2406094. https://doi.org/10.1002/adma.202406094.
6. Yang, S.; Li, Y.; Kang, F.; et al. Recent Progress in Organic Cocrystal-Based Superlattices and Their Optoelectronic Applications. *Adv. Funct. Mater.* **2025**, 2504976. https://doi.org/10.1002/adfm.202504976.
7. Cheema, S.S.; Shanker, N.; Hsu, S.-L.; et al. Giant energy storage and power density negative capacitance superlattices. *Nature* **2024**, *629*, 803–809. https://doi.org/10.1038/s41586-024-07365-5.
8. Lv, J.; Xie, J.; Mohamed, A.G.A.; et al. Photoelectrochemical energy storage materials: Design principles and functional devices towards direct solar to electrochemical energy storage. *Chem. Soc. Rev.* **2022**, *51*, 1511–1528. https://doi.org/10.1039/D1CS00859E.
9. Kment, Š.; Bakandritsos, A.; Tantis, I.; et al. Single Atom Catalysts Based on Earth-Abundant Metals for Energy-Related Applications. *Chem. Rev.* **2024**, *124*, 11767–11847. https://doi.org/10.1021/acs.chemrev.4c00155.
10. Schweidler, S.; Brezesinski, T.; Breitung, B. Entropy-assisted epitaxial coating. *Nat. Energy* **2024**, *9*, 240–241. https://doi.org/10.1038/s41560-024-01468-z.
11. Ju, Z.; Zheng, T.; Zhang, B.; et al. Interfacial chemistry in multivalent aqueous batteries: Fundamentals, challenges, and advances. *Chem. Soc. Rev.* **2024**, *53*, 8980–9028. https://doi.org/10.1039/D4CS00474D.
12. Zhang, W.; Li, Y.; Zhang, C.; et al. Synchronous Regulation of Hydrophobic Molecular Architecture and Interface Engineering for Robust WORM-Type Memristor. *Adv. Funct. Mater.* **2024**, *34*, 2404625. https://doi.org/10.1002/adfm.202404625.
13. Zhang, G.; Feng, W.; Du, G.; et al. Thermodynamically-Driven Phase Engineering and Reconstruction Deduction of Medium-Entropy Prussian Blue Analogue Nanocrystals. *Adv. Mater.* **2025**, 2503814. https://doi.org/10.1002/adma.202503814.
14. Xu, X.; Zhang, Z.; Zhang, Z.; et al. Metalion-bonded two-dimensional framework non-Van der Waals sandwich heterojunctions for fast mass transfer in flexible in-plane micro-supercapacitors. *eScience* **2025**, *in press*. https://doi.org/10.1016/j.esci.2025.100404.
15. Giri, A.; Park, G.; Jeong, U. Layer-Structured Anisotropic Metal Chalcogenides: Recent Advances in Synthesis, Modulation, and Applications. *Chem. Rev.* **2023**, *123*, 3329–3442. https://doi.org/10.1021/acs.chemrev.2c00455.
16. Zhang, P.; Zhang, W.; Wang, Z.; et al. High-voltage, low-temperature supercapacitors enabled by localized "water-in-pyrrolidinium chloride" electrolyte. *eScience* **2023**, *3*, 100184. https://doi.org/10.1016/j.esci.2023.100184.
17. Seenivasan, S.; Adhikari, S.; Sivagurunathan, A.T.; et al. Supercapatteries: Unlocking the potential of battery-supercapacitor fusion. *Energy Environ. Sci.* **2025**, *18*, 1054–1095. https://doi.org/10.1039/D4EE04348K.
18. Pandey, D.; Kumar, K.S.; Thomas, J. Supercapacitor electrode energetics and mechanism of operation: Uncovering the voltage window. *Prog. Mater Sci.* **2024**, *141*, 101219. https://doi.org/10.1016/j.pmatsci.2023.101219.
19. Jing, C.; Tao, S.; Fu, B.; et al. Layered double hydroxide-based nanomaterials for supercapacitors and batteries: Strategies and mechanisms. *Prog. Mater Sci.* **2025**, *150*, 101410. https://doi.org/10.1016/j.pmatsci.2024.101410.
20. Xu, J.; Yuan, X.; Zhao, Y.; et al. One-step hydrothermal synthesis of few-layered metallic phase MoS_2 for high-performance supercapacitors. *Prog. Nat. Sci.-Mater.* **2024**, *34*, 429–436. https://doi.org/10.1016/j.pnsc.2024.04.011.
21. Dong, W.; Xie, M.; Zhao, S.; et al. Materials design and preparation for high energy density and high power density electrochemical supercapacitors. *Mater. Sci. Eng. R Rep.* **2023**, *152*, 100713. https://doi.org/10.1016/j.mser.2022.100713.
22. Zheng, W.; Yang, L.; Zhang, P.; et al. Mass loading and self-discharge challenges for MXene-based aqueous supercapacitors. *Energy Storage Mater.* **2023**, *63*, 103037. https://doi.org/10.1016/j.ensm.2023.103037.
23. Haque, M.; Li, Q.; Rigato, C.; et al. Identification of self-discharge mechanisms of ionic liquid electrolyte based supercapacitor under high-temperature operation. *J. Power Sources* **2021**, *485*, 229328. https://doi.org/10.1016/j.jpowsour.2020.229328.

24. Ramulu, B.; Shaik, J.A.; Mule, A.R.; et al. Improved rate capability and energy density of high-mass hybrid supercapacitor realized through long-term cycling stability testing and selective electrode design. *Mater. Sci. Eng. R Rep.* **2024**, *160*, 100820. https://doi.org/10.1016/j.mser.2024.100820.
25. Flores-Diaz, N.; De Rossi, F.; Das, A.; et al. Progress of Photocapacitors. *Chem. Rev.* **2023**, *123*, 9327–9355. https://doi.org/10.1021/acs.chemrev.2c00773.
26. Zhou, S.; Shekhah, O.; Ramírez, A.; et al. Asymmetric pore windows in MOF membranes for natural gas valorization. *Nature* **2022**, *606*, 706–712. https://doi.org/10.1038/s41586-022-04763-5.
27. Navalón, S.; Dhakshinamoorthy, A.; Álvaro, M.; et al. Metal–Organic Frameworks as Photocatalysts for Solar-Driven Overall Water Splitting. *Chem. Rev.* **2023**, *123*, 445–490. https://doi.org/10.1021/acs.chemrev.2c00460.
28. Gong, W.; Chen, Z.; Dong, J.; et al. Chiral Metal–Organic Frameworks. *Chem. Rev.* **2022**, *122*, 9078–9144. https://doi.org/10.1021/acs.chemrev.1c00740.
29. Chen, T.; Deng, Z.; Lu, W.; et al. Pillar-Supported 2D Layered MOFs with Abundant Active-Site Distributions for High-Performance Alkaline Supercapacitors. *Inorg. Chem.* **2024**, *63*, 18699–18709. https://doi.org/10.1021/acs.inorgchem.4c02479.
30. Xu, D.; Pan, C. Glass formation, structure, relaxation, and property of metal-organic framework (MOF) glasses: A review. *Prog. Nat. Sci.-Mater.* **2025**, *35*, 98–121. https://doi.org/10.1016/j.pnsc.2024.12.006.
31. Yaghi, O.M.; Li, H.L. Hydrothermal Synthesis of a Metal-Organic Framework Containing Large Rectangular Channel. *J. Am. Chem. Soc.* **1995**, *117*, 10401–10402. https://doi.org/10.1021/ja00146a033.
32. Li, H.; Eddaoudi, M.; O'Keeffe, M.; et al. Design and synthesis of an exceptionally stable and highly porous metal-organic framework. *Nature* **1999**, *402*, 276–279. https://doi.org/10.1038/46248.
33. Song, A.-M.; Yang, M.-J.; Wu, Z.; et al. Rational Designed Metal–Organic Framework with Nanocavity Traps for Selectively Recognizing and Separating of Radioactive Thorium in Rare Earth Wastewater. *Adv. Funct. Mater.* **2024**, *34*, 2406932. https://doi.org/10.1002/adfm.202406932.
34. Lamaire, A.; Wieme, J.; Vandenhaute, S.; et al. Water motifs in zirconium metal-organic frameworks induced by nanoconfinement and hydrophilic adsorption sites. *Nat. Commun.* **2024**, *15*, 9997. https://doi.org/10.1038/s41467-024-54358-z.
35. Hu, L.; Wu, W.; Hu, M.; et al. Double-walled Al-based MOF with large microporous specific surface area for trace benzene adsorption. *Nat. Commun.* **2024**, *15*, 3204. https://doi.org/10.1038/s41467-024-47612-x.
36. Wang, Y.; Liu, Z.; Li, J.; et al. Polyaniline-on-MOF protects the MOF structure during carbonization for the construction of a portable sensor to detect tert-butylhydroquinone. *Nano Energy* **2025**, *135*, 110655. https://doi.org/10.1016/j.nanoen.2025.110655.
37. Xiang, Y.; Wei, S.; Wang, T.; et al. Transformation of metal-organic frameworks (MOFs) under different factors. *Coord. Chem. Rev.* **2025**, *523*, 216263. https://doi.org/10.1016/j.ccr.2024.216263.
38. Song, M.; Zhang, Q.; Luo, G.; et al. Coordination structure engineering of single atoms derived from MOFs for Electrocatalysis. *Coord. Chem. Rev.* **2025**, *523*, 216281. https://doi.org/10.1016/j.ccr.2024.216281.
39. Song, G.; Shi, Y.; Jiang, S.; et al. Recent Progress in MOF-Derived Porous Materials as Electrodes for High-Performance Lithium-Ion Batteries. *Adv. Funct. Mater.* **2023**, *33*, 2303121. https://doi.org/10.1002/adfm.202303121.
40. Øien-Ødegaard, S.; Shearer, G.C.; Wragg, D.S.; et al. Pitfalls in metal–organic framework crystallography: Towards more accurate crystal structures. *Chem. Soc. Rev.* **2017**, *46*, 4867–4876. https://doi.org/10.1039/C6CS00533K.
41. Luo, Y.; Bag, S.; Zaremba, O.; et al. MOF Synthesis Prediction Enabled by Automatic Data Mining and Machine Learning. *Angew. Chem. Int. Ed.* **2022**, *61*, e202200242. https://doi.org/10.1002/anie.202200242.
42. Hong, T.; Lee, C.; Bak, Y.; et al. On-Demand Tunable Electrical Conductance Anisotropy in a MOF-Polymer Composite. *Small* **2024**, *20*, 2309469. https://doi.org/10.1002/smll.202309469.
43. Zhang, H.; Zhang, Q.; Zeng, X. Construction of multiple heterogeneous interfaces and oxygen evolution reaction of hollow CoFe bimetallic phosphides derived from MOF template. *Prog. Nat. Sci.-Mater.* **2024**, *34*, 913–920. https://doi.org/10.1016/j.pnsc.2024.09.001.
44. Gao, J.; Hu, Y.; Wang, Y.; et al. MOF Structure Engineering to Synthesize Co-N-C Catalyst with Richer Accessible Active Sites for Enhanced Oxygen Reduction. *Small* **2021**, *17*, 2104684. https://doi.org/10.1002/smll.202104684.
45. Kim, M.; Yi, J.; Park, S.-H.; et al. Heterogenization of Molecular Electrocatalytic Active Sites through Reticular Chemistry. *Adv. Mater.* **2023**, *35*, 2203791. https://doi.org/10.1002/adma.202203791.
46. Zhang, S.; Gao, H.; Xu, X.; et al. MOF-derived CoN/N-C@SiO_2 yolk-shell nanoreactor with dual active sites for highly efficient catalytic advanced oxidation processes. *Chem. Eng. J.* **2020**, *381*, 122670. https://doi.org/10.1016/j.cej.2019.122670.
47. Li, Y.; Guo, Q.; Ding, Z.; et al. MOFs-Based Materials for Solid-State Hydrogen Storage: Strategies and Perspectives. *Chem. Eng. J.* **2024**, *485*, 149665. https://doi.org/10.1016/j.cej.2024.149665.

48. Kim, W.-T.; Lee, W.-G.; An, H.-E.; et al. Machine learning-assisted design of metal–organic frameworks for hydrogen storage: A high-throughput screening and experimental approach. *Chem. Eng. J.* **2025**, *507*, 160766. https://doi.org/10.1016/j.cej.2025.160766.
49. Yang, Z.; Wang, Y.; Lin, X.; et al. Vanadium induces Ni-Co MOF formation from a NiCo LDH to catalytically enhance the MgH2 hydrogen storage performance. *J. Magnes. Alloys* **2025**, *in press*. https://doi.org/10.1016/j.jma.2025.01.012.
50. Kim, D.W.; Jung, M.; Shin, D.Y.; et al. Fine-tuned MOF-74 type variants with open metal sites for high volumetric hydrogen storage at near-ambient temperature. *Chem. Eng. J.* **2024**, *489*, 151500. https://doi.org/10.1016/j.cej.2024.151500.
51. Jin, S. How to Effectively Utilize MOFs for Electrocatalysis. *ACS Energy Lett.* **2019**, *4*, 1443–1445. https://doi.org/10.1021/acsenergylett.9b01134.
52. Li, X.; Zhu, Q.-L. MOF-based materials for photo- and electrocatalytic CO_2 reduction. *EnergyChem* **2020**, *2*, 100033. https://doi.org/10.1016/j.enchem.2020.100033.
53. Mamaghani, A.H.; Liu, J.W.; Zhang, Z.; et al. Promises of MOF-Based and MOF-Derived Materials for Electrocatalytic CO_2 Reduction. *Adv. Energy Mater.* **2024**, *14*, 2402278. https://doi.org/10.1002/aenm.202402278.
54. Chauhan, N.P.S.; Perumal, P.; Chundawat, N.S.; et al. Achiral and chiral metal-organic frameworks (MOFs) as an efficient catalyst for organic synthesis. *Coord. Chem. Rev.* **2025**, *533*, 216536. https://doi.org/10.1016/j.ccr.2025.216536.
55. Sun, N.; Shah, S.S.A.; Lin, Z.; et al. MOF-Based Electrocatalysts: An Overview from the Perspective of Structural Design. *Chem. Rev.* **2025**, *125*, 2703–2792. https://doi.org/10.1021/acs.chemrev.4c00664.
56. Jin, R.; Li, R.; Ma, M.-L.; et al. Beyond Tradition: A MOF-On-MOF Cascade Z-Scheme Heterostructure for Augmented CO_2 Photoreduction. *Small* **2025**, 2409759. https://doi.org/10.1002/smll.202409759.
57. Li, C.; Yan, H.; Yang, H.; et al. Recent advances and future perspectives of metal-organic frameworks as efficient electrocatalysts for CO_2 reduction. *Sci. China Mater.* **2025**, *68*, 21–38. https://doi.org/10.1007/s40843-024-3165-6.
58. Zhang, G.; Li, Y.; Du, G.; et al. Spiral-Concave Prussian Blue Crystals with Rich Steps: Growth Mechanism and Coordination Regulation. *Angew. Chem. Int. Ed.* **2025**, *64*, e202414650. https://doi.org/10.1002/anie.202414650.
59. Ding, M.; Liu, W.; Gref, R. Nanoscale MOFs: From synthesis to drug delivery and theranostics applications. *Adv. Drug Deliver. Rev.* **2022**, *190*, 114496. https://doi.org/10.1016/j.addr.2022.114496.
60. Lázaro, I.A.; Wells, C.J.R.; Forgan, R.S. Multivariate Modulation of the Zr MOF UiO-66 for Defect-Controlled Combination Anticancer Drug Delivery. *Angew. Chem. Int. Ed.* **2020**, *59*, 5211–5217. https://doi.org/10.1002/anie.201915848.
61. Cedrún-Morales, M.; Ceballos, M.; Soprano, E.; et al. Light-Responsive Nanoantennas Integrated into Nanoscale Metal–Organic Frameworks for Photothermal Drug Delivery. *Small Sci.* **2024**, *4*, 2400088. https://doi.org/10.1002/smsc.202400088.
62. Wu, M.X.; Yang, Y.W. Metal–Organic Framework (MOF)-Based Drug/Cargo Delivery and Cancer Therapy. *Adv. Mater.* **2017**, *29*, 1606134. https://doi.org/10.1002/adma.201606134.
63. Yu, Q.; Zhang, Q.; Wu, Z.; et al. Inhalable Metal–Organic Frameworks: A Promising Delivery Platform for Pulmonary Diseases Treatment. *ACS Nano* **2025**, *19*, 3037–3053. https://doi.org/10.1021/acsnano.4c16873.
64. Park, C.; Woo, J.; Jeon, M.; et al. Dual-MOF-Layered Films via Solution Shearing Approach: A Versatile Platform for Tunable Chemiresistive Sensors. *ACS Nano* **2025**, *19*, 11230–11240. https://doi.org/10.1021/acsnano.4c18848.
65. Wang, M.; Zhang, H.; Yan, S.; et al. Fabrication of MOF-based Nanozyme sensor arrays and their application in disease diagnosis. *Coord. Chem. Rev.* **2025**, *532*, 216506. https://doi.org/10.1016/j.ccr.2025.216506.
66. Jang, W.; Yoo, H.; Shin, D.; et al. Colorimetric identification of colorless acid vapors using a metal-organic framework-based sensor. *Nat. Commun.* **2025**, *16*, 385. https://doi.org/10.1038/s41467-024-55774-x.
67. Mohanty, B.; Kumari, S.; Yadav, P.; et al. Metal-organic frameworks (MOFs) and MOF composites based biosensors. *Coord. Chem. Rev.* **2024**, *519*, 216102. https://doi.org/10.1016/j.ccr.2024.216102.
68. Zhang, D.; Wang, W.; Li, S.; et al. Design strategies and energy storage mechanisms of MOF-based aqueous zinc ion battery cathode materials. *Energy Storage Mater.* **2024**, *69*, 103436. https://doi.org/10.1016/j.ensm.2024.103436.
69. Zhou, W.; Tang, Y.; Zhang, X.; et al. MOF derived metal oxide composites and their applications in energy storage. *Coord. Chem. Rev.* **2023**, *477*, 214949. https://doi.org/10.1016/j.ccr.2022.214949.
70. Polyukhov, D.M.; Kudriavykh, N.A.; Gromilov, S.A.; et al. Efficient MOF-Catalyzed Ortho–Para Hydrogen Conversion for Practical Liquefaction and Energy Storage. *ACS Energy Lett.* **2022**, *7*, 4336–4341. https://doi.org/10.1021/acsenergylett.2c02149.
71. Du, R.; Wu, Y.F.; Yang, Y.C.; et al. Porosity Engineering of MOF-Based Materials for Electrochemical Energy Storage. *Adv. Energy Mater.* **2021**, *11*, 2100154. https://doi.org/10.1002/aenm.202100154.
72. Cao, W.; Chen, Z.; Chen, J.; et al. Applications of MOF derivatives based on heterogeneous element doping in the field of electrochemical energy storage. *Mater. Today* **2024**, *77*, 118–141. https://doi.org/10.1016/j.mattod.2024.06.006.

73. Ji, B.; Li, W.; Zhang, F.; et al. MOF-Derived Transition Metal Phosphides for Supercapacitors. *Small* **2025**, *21*, 2409273. https://doi.org/10.1002/smll.202409273.
74. Wang, Y.; Liu, J.; Cao, H.; et al. Facile synthesis of porous high-entropy perovskite nanoparticles through MOF gel method for solid-state supercapacitor application. *Chem. Eng. J.* **2025**, *509*, 161246. https://doi.org/10.1016/j.cej.2025.161246.
75. Cheng, H.; Li, J.; Meng, T.; et al. Advances in Mn-Based MOFs and Their Derivatives for High-Performance Supercapacitor. *Small* **2024**, *20*, 2308804. https://doi.org/10.1002/smll.202308804.
76. Niu, L.; Wu, T.; Chen, M.; et al. Conductive Metal–Organic Frameworks for Supercapacitors. *Adv. Mater.* **2022**, *34*, 2200999. https://doi.org/10.1002/adma.202200999.
77. Li, H.; Liu, Y.; Zhu, X.; et al. Exploring new fields of supercapacitors by regulating metal ions in MOFs. *Energy Storage Mater.* **2024**, *73*, 103859. https://doi.org/10.1016/j.ensm.2024.103859.
78. Cui, S.; Gu, Y.; Tang, Y.; et al. Vacancy engineering regulating specific capacitance of supercapacitors in MOF-on-MOF derived $CoSe_2$ quantum dots embedded in carbon and $CoSe_2$ hollow cages. *Chem. Eng. J.* **2025**, *512*, 162326. https://doi.org/10.1016/j.cej.2025.162326.
79. Yanfei, Z.; Qian, L.; Guangxun, Z.; et al. Recent advances in the type, synthesis and electrochemical application of defective metal-organic frameworks. *Energy Mater.* **2023**, *3*, 300022. https://doi.org/10.20517/energymater.2023.06.
80. Li, S.; Han, W.; An, Q.-F.; et al. Defect Engineering of MOF-Based Membrane for Gas Separation. *Adv. Funct. Mater.* **2023**, *33*, 2303447. https://doi.org/10.1002/adfm.202303447.
81. Ren, J.; Ledwaba, M.; Musyoka, N.M.; et al. Structural defects in metal–organic frameworks (MOFs): Formation, detection and control towards practices of interests. *Coord. Chem. Rev.* **2017**, *349*, 169–197. https://doi.org/10.1016/j.ccr.2017.08.017.
82. Dai, S.; Simms, C.; Patriarche, G.; et al. Highly defective ultra-small tetravalent MOF nanocrystals. *Nat. Commun.* **2024**, *15*, 3434. https://doi.org/10.1038/s41467-024-47426-x.
83. Sk, S.; Islam, H.; Abraham, B.M.; et al. Defects in MOFs for Photocatalytic Water Reduction to Hydrogen Generation: From Fundamental Understanding to State-of-Art Materials. *Small Methods* **2024**, 2401689. https://doi.org/10.1002/smtd.202401689.
84. Zhang, C.; Han, C.; Sholl, D.S.; et al. Computational Characterization of Defects in Metal–Organic Frameworks: Spontaneous and Water-Induced Point Defects in ZIF-8. *J. Phys. Chem. Lett.* **2016**, *7*, 459–464. https://doi.org/10.1021/acs.jpclett.5b02683.
85. Park, H.; Kim, S.; Jung, B.; et al. Defect Engineering into Metal–Organic Frameworks for the Rapid and Sequential Installation of Functionalities. *Inorg. Chem.* **2018**, *57*, 1040–1047. https://doi.org/10.1021/acs.inorgchem.7b02391.
86. An, H.; Tian, W.; Lu, X.; et al. Boosting the CO_2 adsorption performance by defect-rich hierarchical porous Mg-MOF-74. *Chem. Eng. J.* **2023**, *469*, 144052. https://doi.org/10.1016/j.cej.2023.144052.
87. Chen, T.; Xu, H.; Li, S.; et al. Tailoring the Electrochemical Responses of MOF-74 via Dual-Defect Engineering for Superior Energy Storage. *Adv. Mater.* **2024**, *36*, 2402234. https://doi.org/10.1002/adma.202402234.
88. Gu, Y.; Anjali, B.A.; Yoon, S.; et al. Defect-engineered MOF-801 for cycloaddition of CO_2 with epoxides. *J. Mater. Chem. A* **2022**, *10*, 10051–10061. https://doi.org/10.1039/D2TA00503D.
89. Liang, S.; Xiao, X.; Bai, L.; et al. Conferring Ti-Based MOFs with Defects for Enhanced Sonodynamic Cancer Therapy. *Adv. Mater.* **2021**, *33*, 2100333. https://doi.org/10.1002/adma.202100333.
90. Wu, J.; Dai, Q.; Zhang, H.; et al. A defect-free MOF composite membrane prepared via in-situ binder-controlled restrained second-growth method for energy storage device. *Energy Storage Mater.* **2021**, *35*, 687–694. https://doi.org/10.1016/j.ensm.2020.11.040.
91. Lu, Y.; Zhou, R.; Wang, N.; et al. Engineer Nanoscale Defects into Selective Channels: MOF-Enhanced Li^+ Separation by Porous Layered Double Hydroxide Membrane. *Nano-Micro Lett.* **2023**, *15*, 147. https://doi.org/10.1007/s40820-023-01101-w.
92. Sepehrmansourie, H.; Alamgholiloo, H.; Noroozi Pesyan, N.; et al. A MOF-on-MOF strategy to construct double Z-scheme heterojunction for high-performance photocatalytic degradation. *Appl. Catal. B-Environ.* **2023**, *321*, 122082. https://doi.org/10.1016/j.apcatb.2022.122082.
93. Guan, Y.; Liu, T.; Wu, Y.; et al. Modulating the electronic structure of Ru using a self-reconstructed MOF-NiFeOOH heterointerface for improved electrocatalytic water splitting. *J. Mater. Chem. A* **2024**, *12*, 17404–17412. https://doi.org/10.1039/D4TA02569E.
94. Wang, Y.; Haidry, A.A.; Liu, Y.; et al. Enhanced electromagnetic wave absorption using bimetallic MOFs-derived TiO_2/Co/C heterostructures. *Carbon* **2024**, *216*, 118497. https://doi.org/10.1016/j.carbon.2023.118497.
95. Li, K.; Liu, Z.-T.; Liu, Z.-W.; et al. Fast Photo- and Moisture-Driven Bidirectional Actuation of a Shape-Programmable MOF Loading Composite. *Chem. Eng. J.* **2025**, *506*, 159503. https://doi.org/10.1016/j.cej.2025.159503.

96. Wang, K.; Chen, C.; Li, Y.; et al. Insight into Electrochemical Performance of Nitrogen-Doped Carbon/NiCo-Alloy Active Nanocomposites. *Small* **2023**, *19*, 2300054. https://doi.org/10.1002/smll.202300054.
97. Deng, Z.; Wang, L.; Chen, T.; et al. Stable metal-organic frameworks with Zr_6 clusters for alkaline battery-supercapacitor devices. *J. Solid State Chem.* **2024**, *340*, 125009. https://doi.org/10.1016/j.jssc.2024.125009.
98. Wang, Y.; Lu, W.; Wang, L.; et al. Vanadate-based Fe-MOFs as promising negative electrode for hybrid supercapacitor device. *Nanotechnology* **2024**, *35*, 205402. https://doi.org/10.1088/1361-6528/ad1d12.
99. Yu, X.; Hu, Y.; Luan, X.; et al. Microwave-assisted construction of MXene/MOF aerogel via N-metal bonds for efficient photodegradation of vapor acetone under high humidity. *Chem. Eng. J.* **2023**, *476*, 146878. https://doi.org/10.1016/j.cej.2023.146878.
100. Chen, Q.; Xue, Z.; Wei, F.; et al. Microwave-assisted rapid controllable synthesis of hexagonal prismatic CoNi-MOF-74 and its derivative for efficient oxygen evolution reaction. *Int. J. Hydrogen Energy* **2024**, *51*, 1327–1336. https://doi.org/10.1016/j.ijhydene.2023.11.081.
101. Yahia, M.; Lozano, L.A.; Zamaro, J.M.; et al. Microwave-assisted synthesis of metal–organic frameworks UiO-66 and MOF-808 for enhanced CO_2/CH_4 separation in PIM-1 mixed matrix membranes. *Sep. Purif. Technol.* **2024**, *330*, 125558. https://doi.org/10.1016/j.seppur.2023.125558.
102. Fan, J.; Wu, W.; Lu, Z.; et al. Rapid synthesis strategy of ultrathin UiO-66 separation membranes: Ultrasonic-assisted nucleation followed with microwave-assisted growth. *J. Membr. Sci.* **2022**, *664*, 121085. https://doi.org/10.1016/j.memsci.2022.121085.
103. Li, Q.; Liu, Y.; Niu, S.; et al. Microwave-assisted rapid synthesis and activation of ultrathin trimetal–organic framework nanosheets for efficient electrocatalytic oxygen evolution. *J. Colloid Interface Sci.* **2021**, *603*, 148–156. https://doi.org/10.1016/j.jcis.2021.06.102.
104. Wen, M.; Sun, N.; Jiao, L.; et al. Microwave-Assisted Rapid Synthesis of MOF-Based Single-Atom Ni Catalyst for CO_2 Electroreduction at Ampere-Level Current. *Angew. Chem. Int. Ed.* **2024**, *63*, e202318338. https://doi.org/10.1002/anie.202318338.
105. Asghar, A.; Iqbal, N.; Noor, T.; et al. Efficient electrochemical synthesis of a manganese-based metal–organic framework for H_2 and CO_2 uptake. *Green Chem.* **2021**, *23*, 1220–1227. https://doi.org/10.1039/D0GC03292A.
106. Wu, W.; Decker, G.E.; Weaver, A.E.; et al. Facile and Rapid Room-Temperature Electrosynthesis and Controlled Surface Growth of Fe-MIL-101 and Fe-MIL-101-NH_2. *ACS Cent. Sci.* **2021**, *7*, 1427–1433. https://doi.org/10.1021/acscentsci.1c00686.
107. Pei, Z.; Guo, Y.; Luan, D.; et al. Regulating the Local Reaction Microenvironment at Chromium Metal–Organic Frameworks for Efficient H_2O_2 Electrosynthesis in Neutral Electrolytes. *Adv. Mater.* **2025**, *37*, 2500274. https://doi.org/10.1002/adma.202500274.
108. Tang, D.; Yang, X.; Wang, B.; et al. One-Step Electrochemical Growth of 2D/3D Zn(II)-MOF Hybrid Nanocomposites on an Electrode and Utilization of a PtNPs@2D MOF Nanocatalyst for Electrochemical Immunoassay. *ACS Appl. Mater. Inter.* **2021**, *13*, 46225–46232. https://doi.org/10.1021/acsami.1c09095.
109. Wei, H.; Qin, F. Electrochemical Synthesis and Conductivity Fine Tuning of the 2D Iron-Quinoid Metal–Organic Framework. *ACS Appl. Mater. Inter.* **2025**, *17*, 2010–2017. https://doi.org/10.1021/acsami.4c17699.
110. Cliffe, M.J.; Hill, J.A.; Murray, C.A.; et al. Defect-dependent colossal negative thermal expansion in UiO-66(Hf) metal-organic framework. *Phys. Chem. Chem. Phys.* **2015**, *17*, 11586–11592. https://doi.org/10.1039/c5cp01307k.
111. Ren, J.W.; Rogers, D.E.C.; Segakweng, T.; et al. Thermal treatment induced transition from $Zn_3(OH)_2(BDC)_2$ (MOF-69c) to $Zn_4O(BDC)_3$(MOF-5). *Int. J. Mater. Res.* **2014**, *105*, 89–93. https://doi.org/10.3139/146.110994.
112. Borges, D.D.; Devautour-Vinot, S.; Jobic, H.; et al. Proton Transport in a Highly Conductive Porous Zirconium-Based Metal-Organic Framework: Molecular Insight. *Angew. Chem. Int. Ed.* **2016**, *55*, 3919–3924. https://doi.org/10.1002/anie.201510855.
113. Zhang, Y.; Liu, J.J.; Zhang, L.; et al. Particle shape characterisation and classification using automated microscopy and shape descriptors in batch manufacture of particulate solids. *Particuology* **2016**, *24*, 61–68. https://doi.org/10.1016/j.partic.2014.12.012.
114. Wu, D.; Yan, W.; Xu, H et al. Defect engineering of Mn-based MOFs with rod-shaped building units by organic linker fragmentation. *Inorg. Chim. Acta* **2017**, *460*, 93–98. https://doi.org/10.1016/j.ica.2016.07.022.
115. Wang, X.; Zhang, X.; Zhao, Y.; et al. Accelerated Multi-step Sulfur Redox Reactions in Lithium-Sulfur Batteries Enabled by Dual Defects in Metal-Organic Framework-based Catalysts. *Angew. Chem. Int. Ed.* **2023**, *62*, e202306901. https://doi.org/10.1002/anie.202306901.
116. Wang, Z.-D.; Zang, Y.; Liu, Z.-J.; et al. Opening catalytic sites in the copper-triazoles framework via defect chemistry for switching on the proton reduction. *Appl. Catal. B-Environ.* **2021**, *288*, 119941. https://doi.org/10.1016/j.apcatb.2021.119941.

117. Salman, M.; Qin, H.; Zou, Y.; et al. In-situ decoration of NiCo-thiophene based metal-organic framework on nickel foam as an efficient electrocatalyst for oxygen evolution reaction. *J. Power Sources* **2025**, *629*, 235942. https://doi.org/10.1016/j.jpowsour.2024.235942.
118. Li, W.-Q.; Li, Y.-M.; Hou, N.; et al. Hydroxyl-induced structural defects in metal-organic frameworks for improved photocatalytic decontamination: Accelerated exciton dissociation and hydrogen bonding interaction. *J. Hazard. Mater.* **2025**, *487*, 137149. https://doi.org/10.1016/j.jhazmat.2025.137149.
119. Dong, Y.; Jin, Z.; Peng, H.; et al. Size Effect and Interfacial Synergy Enhancement of 2D Ultrathin Co_xZn_{1-x}-MOF/rGO for Boosting Lithium–Sulfur Battery Performance. *Small* **2025**, *21*, 2412186. https://doi.org/10.1002/smll.202412186.
120. Liu, P.; Lyu, J.; Bai, P. Synthesis of mixed matrix membrane utilizing robust defective MOF for size-selective adsorption of dyes. *Sep. Purif. Technol.* **2025**, *354*, 128672. https://doi.org/10.1016/j.seppur.2024.128672.
121. Liu, Z.; Zhao, H.; Hua, B.; et al. Ionic Liquid-Functionalized Defective MOFs for Membrane-Based CO_2 Separation: A Dual Optimization Approach for Interface and Transport. *ACS Appl. Mater. Inter.* **2025**, *17*, 6867–6877. https://doi.org/10.1021/acsami.4c16340.
122. Hou, X.; Wang, J.; Mousavi, B.; et al. Strategies for induced defects in metal–organic frameworks for enhancing adsorption and catalytic performance. *Dalton Trans.* **2022**, *51*, 8133–8159. https://doi.org/10.1039/D2DT01030E.
123. Chang, Y.-N.; Shen, C.-H.; Huang, C.-W.; et al. Defective Metal–Organic Framework Nanocrystals as Signal Amplifiers for Electrochemical Dopamine Sensing. *ACS Appl. Nano Mater.* **2023**, *6*, 3675–3684. https://doi.org/10.1021/acsanm.2c05402.
124. Cheng, W.; Ren, X.; Wang, X.; et al. Improving the Photoactivity of Porphyrin-Based Metal–Organic Frameworks via Constructing [Ce–O] Active Site and Vacancy. *Inorg. Chem.* **2024**, *63*, 14050–14061. https://doi.org/10.1021/acs.inorgchem.4c01836.
125. Baumann, A.E.; Burns, D.A.; Díaz, J.C.; et al. Lithiated Defect Sites in Zr Metal–Organic Framework for Enhanced Sulfur Utilization in Li–S Batteries. *ACS Appl. Mater. Inter.* **2019**, *11*, 2159–2167. https://doi.org/10.1021/acsami.8b19034.
126. Chen, T.; Bian, S.; Yang, X.; et al. A hollow urchin-like metal–organic framework with Ni–O-cluster SBUs as a promising electrode for an alkaline battery–supercapacitor device. *Inorg. Chem. Front.* **2023**, *10*, 2380–2386. https://doi.org/10.1039/D3QI00123G.
127. Xu, Z.; Lv, B.; Shi, X.; et al. Chemical transformation of hollow coordination polymer particles to Co_3O_4 nanostructures and their pseudo-capacitive behaviors. *Inorg. Chim. Acta* **2015**, *427*, 266–272. https://doi.org/10.1016/j.ica.2015.01.008.
128. Li, M.; Wang, J.; Wang, F.; et al. Construction of internal and external defect electrode materials based on hollow manganese-cobalt-nickel sulfide nanotube arrays. *Appl. Surf. Sci.* **2021**, *568*, 150900. https://doi.org/10.1016/j.apsusc.2021.150900.
129. Wang, K.-B.; Xun, Q.; Zhang, Q. Recent progress in metal-organic frameworks as active materials for supercapacitors. *EnergyChem* **2020**, *2*, 100025. https://doi.org/10.1016/j.enchem.2019.100025.
130. Wang, K.; Bi, R.; Huang, M.; et al. Porous Cobalt Metal–Organic Frameworks as Active Elements in Battery–Supercapacitor Hybrid Devices. *Inorg. Chem.* **2020**, *59*, 6808–6814. https://doi.org/10.1021/acs.inorgchem.0c00060.
131. Li, J.; Zhao, L.; Liu, P. Facile electrodepositing coral-/urchin-like polyaniline on carbon cloth in salty media as electrode for high-performance flexible supercapacitors. *Prog. Nat. Sci-Mater.* **2023**, *33*, 668–673. https://doi.org/10.1016/j.pnsc.2023.11.012.
132. Wang, L.; Fu, R.; Qi, X.; et al. Deashing Strategy on Biomass Carbon for Achieving High-Performance Full-Supercapacitor Electrodes. *ACS Appl. Mater. Interfaces* **2024**, *16*, 52663–52673. https://doi.org/10.1021/acsami.4c11778.
133. Wang, K.; Shi, X.; Zhang, Z.; et al. Size-dependent capacitance of NiO nanoparticles synthesized from Ni-based coordination polymer precursors with different crystallinity. *J. Alloys Compd.* **2015**, *632*, 361–367. https://doi.org/10.1016/j.jallcom.2015.01.252.
134. Liu, L.; Tian, Q.; Yao, W.; et al. All-printed ultraflexible and stretchable asymmetric in-plane solid-state supercapacitors (ASCs) for wearable electronics. *J. Power Sources* **2018**, *397*, 59–67. https://doi.org/10.1016/j.jpowsour.2018.07.013.
135. Deng, T.; Lu, Y.; Zhang, W.; et al. Inverted Design for High-Performance Supercapacitor Via $Co(OH)_2$-Derived Highly Oriented MOF Electrodes. *Adv. Energy Mater.* **2018**, *8*, 1702294. https://doi.org/10.1002/aenm.201702294.
136. Fawad Khan, M.; Ali Marwat, M.; Abdullah; Shaheen Shah, S.; et al. Novel MoS_2-sputtered NiCoMg MOFs for high-performance hybrid supercapacitor applications. *Sep. Purif. Technol.* **2023**, *310*, 123101. https://doi.org/10.1016/j.seppur.2023.123101.
137. Dennyson Savariraj, A.; Justin Raj, C.; Kale, A.M.; et al. Road Map for In Situ Grown Binder-Free MOFs and Their Derivatives as Freestanding Electrodes for Supercapacitors. *Small* **2023**, *19*, 2207713. https://doi.org/10.1002/smll.202207713.

138. Wulan Septiani, N.L.; Wustoni, S.; Failamani, F.; et al. Revealing the effect of cobalt content and ligand exchange in the bimetallic Ni–Co MOF for stable supercapacitors with high energy density. *J. Power Sources* **2024**, *603*, 234423. https://doi.org/10.1016/j.jpowsour.2024.234423.
139. Hong, Y.; Chen, T.; Wang, K.; et al. Supercapacitive study for electrode materials around the framework-collapse point of a Ni-based coordination polymer. *CrystEngComm* **2023**, *25*, 122–129. https://doi.org/10.1039/D2CE01236G.
140. Kang, L.; Zhang, M.; Zhang, J.; et al. Dual-defect surface engineering of bimetallic sulfide nanotubes towards flexible asymmetric solid-state supercapacitors. *J. Mater. Chem. A* **2020**, *8*, 24053–24064. https://doi.org/10.1039/D0TA08979F.
141. Darabi, R.; Karimi-Maleh, H. Hierarchical copper-1,3,5 benzenetricarboxylic acid-MOF-derived with nitrogen-doped graphene nanoribbons as a novel assembly nanocomposite for asymmetric supercapacitors. *Adv. Compos. Hybrid Mater.* **2023**, *6*, 114. https://doi.org/10.1007/s42114-023-00696-3.
142. Feng, W.; Liu, C.; Liu, Z.; et al. In-situ growth of N-doped graphene-like carbon/MOF nanocomposites for high-performance supercapacitor. *Chin. Chem. Lett.* **2024**, *35*, 109552. https://doi.org/10.1016/j.cclet.2024.109552.
143. Sun, Z.; Wang, Y.; Yang, L.; et al. RGO-Induced Flower-like Ni-MOF In Situ Self-Assembled Electrodes for High-Performance Hybrid Supercapacitors. *ACS Appl. Mater. Inter.* **2024**, *16*, 584–593. https://doi.org/10.1021/acsami.3c14046.
144. Feng, C.; An, Q.; Zhang, Q.; et al. Unleashing the potential of Ru/FeCo-MOF in water splitting and supercapacitors through Morphology and electronic structure control. *Int. J. Hydrogen Energy* **2024**, *55*, 189–198. https://doi.org/10.1016/j.ijhydene.2023.11.134.
145. Muthu, D.; Dharman, R.K.; Muthu, S.E.; et al. Recent developments in metal-organic framework-derived transition metal oxide@carbon nanostructure and carbon nanostructure for supercapacitor applications. *J. Energy Storage* **2025**, *119*, 116365. https://doi.org/10.1016/j.est.2025.116365.
146. Wang, J.; Li, S.; Fu, N.; et al. MOF-derived carbon-coated NiS/NiS_2 yolk-shell spheres as a satisfactory positive electrode material for hybrid supercapacitors. *Adv. Compos. Hybrid Mater.* **2025**, *8*, 190. https://doi.org/10.1007/s42114-025-01257-6.
147. Wang, K.; Cao, X.; Wang, S.; et al. Interpenetrated and Polythreaded CoII-Organic Frameworks as a Supercapacitor Electrode Material with Ultrahigh Capacity and Excellent Energy Delivery Efficiency. *ACS Appl. Mater. Interfaces* **2018**, *10*, 9104–9115. https://doi.org/10.1021/acsami.7b16141.
148. Helal, A.; Yamani, Z.H.; Cordova, K.E.; et al. Multivariate metal-organic frameworks. *Natl. Sci. Rev.* **2017**, *4*, 296–298. https://doi.org/10.1093/nsr/nwx013.
149. Dong, W.; Liu, Z.; Sun, H.; et al. Ultrathin defect-rich nanosheets of NiFe-MOF with high specific capacitance and stability for supercapacitor. *Mater. Today Chem.* **2024**, *36*, 101938. https://doi.org/10.1016/j.mtchem.2024.101938.
150. Patil, S.A.; Katkar, P.K.; Kaseem, M.; et al. Cu@Fe-Redox Capacitive-Based Metal-Organic Framework Film for a High-Performance Supercapacitor Electrode. *Nanomaterials* **2023**, *13*, 1587. https://doi.org/10.3390/nano13101587.
151. Wang, H.; Liang, M.; Miao, Z. Engineering accordion-like Fe-doped NiS_2 enabling high-performance aqueous supercapacitors and Zn-Ni batteries. *Chem. Eng. J.* **2023**, *470*, 144148. https://doi.org/10.1016/j.cej.2023.144148.
152. Bu, R.; Wang, Y.; Zhao, Y.; et al. "One-for-two" strategy: The construction of high performance positive and negative electrode materials via one Co-based metal organic framework precursor for boosted hybrid supercapacitor energy density. *J. Power Sources* **2022**, *541*, 231689. https://doi.org/10.1016/j.jpowsour.2022.231689.
153. Ren, H.; Guo, H.; Hao, Y.; et al. Defect-regulated MnS@$Ni_{0.654}Co_{0.155}Se_{1.234}S_{0.101}$ structures: A novel approach to unlock energy storage potential in supercapacitors. *J. Colloid Interface Sci.* **2025**, *683*, 746–758. https://doi.org/10.1016/j.jcis.2024.12.225.
154. Cao, Y.; Tian, Z.; Xiang, C.; et al. Se-doped cobalt-nickel sulfide hollow nanospheres with heterostructure and engineered defects as high-performance electrode for supercapacitors. *J. Energy Storage* **2024**, *100*, 113755. https://doi.org/10.1016/j.est.2024.113755.
155. Cui, S.; Tang, Y.; Cui, W.; et al. Simultaneously Improving Energy Storage and Oxygen Evolution Reaction by Causing Regional Defects in MOF-on-MOF Derived Hollow Se-Doped CoP-Fe2P Heterojunctions. *ACS Appl. Mater. Inter.* **2024**, *16*, 42230–42241. https://doi.org/10.1021/acsami.4c08244.
156. Nwaji, N.; Gwak, J.; Goddati, M.; et al. Defect-Engineered Fe_3C@$NiCo_2S_4$ Nanospike Derived from Metal–Organic Frameworks as an Advanced Electrode Material for Hybrid Supercapacitors. *ACS Appl. Mater. Inter.* **2023**, *15*, 34779–34788. https://doi.org/10.1021/acsami.3c04635.
157. Mei, H.; Mei, Y.; Zhang, S.; et al. Bimetallic-MOF Derived Accordion-like Ternary Composite for High-Performance Supercapacitors. *Inorg. Chem.* **2018**, *57*, 10953–10960. https://doi.org/10.1021/acs.inorgchem.8b01574.
158. Liu, S.; Kang, L.; Zhang, J.; et al. Structural engineering and surface modification of MOF-derived cobalt-based hybrid nanosheets for flexible solid-state supercapacitors. *Energy Storage Mater.* **2020**, *32*, 167–177. https://doi.org/10.1016/j.ensm.2020.07.017.

159. Sun, J.; Xue, H.; Zhang, Y.; et al. Unraveling the Synergistic Effect of Heteroatomic Substitution and Vacancy Engineering in $CoFe_2O_4$ for Superior Electrocatalysis Performance. *Nano Lett.* **2022**, *22*, 3503–3511. https://doi.org/10.1021/acs.nanolett.1c04425.
160. Xu, J.; Ge, L.; Zhou, Y.; et al. Insights into N, P, S multi-doped Mo_2C/C composites as highly efficient hydrogen evolution reaction catalysts. *Nanoscale Adv.* **2020**, *2*, 3334–3340. https://doi.org/10.1039/D0NA00335B.
161. Xu, Z.; Teng, R.; Xu, L.; et al. Assembly of Amorphizing Porous Bimetallic Metal-Organic Frameworks Spheres with Zn-O-Fe Cluster and Coordination Deficiency via Ligand Competition for Efficient Electro-Fenton Catalysis. *Adv. Funct. Mater.* **2024**, *34*, 2401248. https://doi.org/10.1002/adfm.202401248.
162. Shearer, G.C.; Chavan, S.; Bordiga, S.; et al. Defect Engineering: Tuning the Porosity and Composition of the Metal–Organic Framework UiO-66 via Modulated Synthesis. *Chem. Mater.* **2016**, *28*, 3749–3761. https://doi.org/10.1021/acs.chemmater.6b00602.
163. Yue, M.L.; Yu, C.Y.; Duan, H.H.; et al. Six Isomorphous Window-Beam MOFs: Explore the Effects o f Metal Ions on MOF-Derived Carbon for Supercapacitors. *Chem. Eur. J.* **2018**, *24*, 16160–16169. https://doi.org/10.1002/chem.201803554.
164. Zhang, H.; Yang, Y.; Deng, Y.; et al. Construction of 2D MOF nanosheets with missing-linker defects for enhanced supercapacitor performance. *J. Alloys Compd.* **2024**, *999*, 175049. https://doi.org/10.1016/j.jallcom.2024.175049.
165. Lin, S.; Guo, X.; Cai, W.; et al. Binder-Free Defective Bimetallic Metal-Organic Framework Nanostructures with Lattice Distortion as Hybrid Supercapacitor Electrodes. *ACS Appl. Nano Mater.* **2024**, *7*, 1078–1088. https://doi.org/10.1021/acsanm.3c05037.
166. Ferhi, N.; Desalegn Assresahegn, B.; Ardila-Suarez, C.; et al. Defective Metal–Organic Framework-808@Polyaniline Composite Materials for High Capacitance Retention Supercapacitor Electrodes. *ACS Appl. Energy Mater.* **2022**, *5*, 1235–1243. https://doi.org/10.1021/acsaem.1c03649.
167. Wang, J.; Deng, S.-Q.; Zhao, T.-T.; et al. A Mn(ii)–MOF with inherent missing metal-ion defects based on an imidazole-tetrazole tripodal ligand and its application in supercapacitors. *Dalton Trans.* **2020**, *49*, 12150–12155. https://doi.org/10.1039/D0DT01666G.
168. Salehi Rozveh, Z.; Pooriraj, M.; Rad, M.; et al. Synergistic effect of metal node engineering and mixed-linker-architected on the energy storage activities of pillar-layered $Cu_2(L)_2$(DABCO) metal-organic frameworks. *Mater. Chem. Phys.* **2022**, *292*, 126761. https://doi.org/10.1016/j.matchemphys.2022.126761.
169. Zhong, W.; Zhao, R.; Zhu, Y.; et al. Vacancy Engineering on MnSe Cathode Enables High-Rate and Stable Zinc-Ion Storage. *Adv. Funct. Mater.* **2024**, *35*, 2419720. https://doi.org/10.1002/adfm.202419720.
170. Sun, M.; Guo, W.; Wang, J.; et al. Microenvironment Reconstitution-Induced Collaborative Oxyanions-Vacancies Engineering for Enhanced High-Mass-Loading Energy Storage. *Adv. Funct. Mater.* **2024**, *34*, 2405116. https://doi.org/10.1002/adfm.202405116.
171. Shi, W.; Meng, Z.; Xu, Z.; et al. Controllable vacancy strategy mediated by organic ligands of nickel fluoride alkoxides for high-performance aqueous energy storage. *J. Mater. Chem. A* **2023**, *11*, 1369–1379. https://doi.org/10.1039/D2TA08004D.
172. Zhang, N.; Yin, L.; Chen, L.; et al. Size- and crystallinity-dependent oxygen vacancy engineering to modulate Fe active sites for enhanced reversible nitrogen fixation in Lithium-nitrogen batteries. *Energy Storage Mater.* **2025**, *76*, 104171. https://doi.org/10.1016/j.ensm.2025.104171.
173. Zhang, D.; Gao, H.; Li, J.; et al. Plasma-enhanced vacancy engineering for sustainable high-performance recycled silicon in lithium-ion batteries. *Energy Storage Mater.* **2025**, *77*, 104231. https://doi.org/10.1016/j.ensm.2025.104231.
174. Cheng, C.; Zhuo, Z.; Xia, X.; et al. Stabilized Oxygen Vacancy Chemistry toward High-Performance Layered Oxide Cathodes for Sodium-Ion Batteries. *ACS Nano* **2024**, *18*, 35052–35065. https://doi.org/10.1021/acsnano.4c14724.
175. Zhu, F.; Sun, L.; Liu, Y.; et al. Dual-defect site regulation on MOF-derived P-Co_3O_4@NC@O_v-NiMnLDH carbon arrays for high-performance supercapacitors. *J. Mater. Chem. A* **2022**, *10*, 21021–21030. https://doi.org/10.1039/D2TA05146J.
176. Wei, J.; Hu, F.; Lv, C.; et al. A surface defect strategy of NiCo-layered double hydroxide decorated MXene layers for durable solid-state supercapacitors. *Mater. Chem. Front.* **2024**, *8*, 3231–3241. https://doi.org/10.1039/D4QM00481G.
177. Chettiannan, B.; Mathan, S.; Arumugam, G.; et al. Attaining high energy density using metal-organic framework-derived NiO/Co_3O_4/$NiCo_2O_4$ as an electrode in asymmetric hybrid supercapacitor. *J. Energy Storage* **2024**, *77*, 110008. https://doi.org/10.1016/j.est.2023.110008.
178. Guo, X.; Liu, Y.; Feng, L.; et al. Zn-substituted Co_3O_4 crystal anchored on porous carbon nanofibers for high performance supercapacitors. *Surf. Interf.* **2024**, *53*, 105048. https://doi.org/10.1016/j.surfin.2024.105048.
179. Xu, D.; Xue, Z.; Han, L.; et al. Interface engineered Zn/Co-S@CeO_2 heterostructured nanosheet arrays as efficient electrodes for supercapacitors. *J. Alloys Compd.* **2023**, *946*, 169399. https://doi.org/10.1016/j.jallcom.2023.169399.
180. Chen, C.; Zhang, H.; Yan, R.; et al. Defect engineering induced nanostructure changes of NiMo-layered double hydroxides/MOF heterostructure on battery type charge storage. *J. Power Sources* **2025**, *639*, 236685. https://doi.org/10.1016/j.jpowsour.2025.236685.

181. Mofokeng, T.P.; Ipadeola, A.K.; Tetana, Z.N.; et al. Defect-Engineered Nanostructured Ni/MOF-Derived Carbons for an Efficient Aqueous Battery-Type Energy Storage Device. *ACS Omega* **2020**, *5*, 20461–20472. https://doi.org/10.1021/acsomega.0c02563.
182. Yang, S.; Qian, L.; Ping, Y.; et al. Electrochemical performance of Bi_2O_3 supercapacitors improved by surface vacancy defects. *Ceram. Int.* **2021**, *47*, 8290–8299. https://doi.org/10.1016/j.ceramint.2020.11.190.
183. Wei, G.; Zhou, Z.; Zhao, X.; et al. Ultrathin Metal–Organic Framework Nanosheet-Derived Ultrathin Co_3O_4 Nanomeshes with Robust Oxygen-Evolving Performance and Asymmetric Supercapacitors. *ACS Appl. Mater. Inter.* **2018**, *10*, 23721–23730. https://doi.org/10.1021/acsami.8b04026.
184. Wang, G.; Jin, Z. Oxygen-vacancy-rich cobalt–aluminium hydrotalcite structures served as high-performance supercapacitor cathode. *J. Mater. Chem. C* **2021**, *9*, 620–632. https://doi.org/10.1039/D0TC03640D.
185. Wei, J.; Hu, F.; Pan, Y.; et al. Design strategy for metal–organic framework assembled on modifications of MXene layers for advanced supercapacitor electrodes. *Chem. Eng. J.* **2024**, *481*, 148793. https://doi.org/10.1016/j.cej.2024.148793.
186. Li, T.; Hu, Y.; Zhang, J.; et al. Doping effect and oxygen vacancy engineering in nickel-manganese layered double hydroxides for high-performance supercapacitors. *Nano Energy* **2024**, *126*, 109690. https://doi.org/10.1016/j.nanoen.2024.109690.
187. Tang, Y.Q.; Shen, H.M.; Cheng, J.Q et al. Fabrication of Oxygen-Vacancy Abundant NiMn-Layered Double Hydroxides for Ultrahigh Capacity Supercapacitors. *Adv. Funct. Mater.* **2020**, *30*, 1908223. https://doi.org/10.1002/adfm.201908223.
188. Chen, X.; Zhang, Z.; Zhou, S.; et al. In-situ growth transformation and oxygen vacancy synergistic modulation of the electronic structure of NiCo-LDH enables high-performance hybrid supercapacitors. *Appl. Energy* **2024**, *371*, 123670. https://doi.org/10.1016/j.apenergy.2024.123670.
189. Zhi, Z.; Wang, J.; Zhou, J.; et al. Oxygen vacancies are generated in the inner layer of the core-shell structure by in-situ electrochemical activation to promote electrochemical energy storage. *J. Energy Storage* **2024**, *100*, 113528. https://doi.org/10.1016/j.est.2024.113528.
190. Chen, K.; Yuan, X.; Tian, Z.; et al. A facile approach for generating ordered oxygen vacancies in metal oxides. *Nat. Mater.* **2025**, *24*, 835–842. https://doi.org/10.1038/s41563-025-02171-4.
191. Guo, J.; Zhao, H.; Yang, Z.; et al. Bimetallic Sulfides with Vacancy Modulation Exhibit Enhanced Electrochemical Performance. *Adv. Funct. Mater.* **2024**, *34*, 2315714. https://doi.org/10.1002/adfm.202315714.
192. Wang, X.; Zhou, R.; Zhang, C et al. Plasma-induced on-surface sulfur vacancies in $NiCo_2S_4$ enhance the energy storage performance of supercapatteries. *J. Mater. Chem. A* **2020**, *8*, 9278–9291. https://doi.org/10.1039/D0TA01991G.
193. Wang, Q.; Qu, Z.; Chen, S.; et al. Metal organic framework derived P-doping CoS@C with sulfide defect to boost high-performance asymmetric supercapacitors. *J. Colloid Interface Sci.* **2022**, *624*, 385–393. https://doi.org/10.1016/j.jcis.2022.03.053.
194. Nwaji, N.; Kang, H.; Goddati, M.; et al. Sulphur vacancy induced Co_3S_4@$CoMo_2S_4$ nanocomposites as a functional electrode for high performance supercapacitors. *J. Mater. Chem. A* **2023**, *11*, 3640–3652. https://doi.org/10.1039/D2TA08820G.
195. Chen, Y.; Guo, H.; Yang, F.; et al. Metal-organic frameworks (MOFs) derived hollow microspheres with rich sulfur vacancies for hybrid supercapacitors. *Electrochim. Acta* **2022**, *434*, 141319. https://doi.org/10.1016/j.electacta.2022.141319.
196. Huang, C.; Gao, A.; Yi, F.; et al. Metal organic framework derived hollow NiS@C with S-vacancies to boost high-performance supercapacitors. *Chem. Eng. J.* **2021**, *419*, 129643. https://doi.org/10.1016/j.cej.2021.129643.
197. Lai, K.; Sun, Y.; Li, N.; et al. Photocatalytic CO_2-to-CH_4 Conversion with Ultrahigh Selectivity of 95.93% on S-Vacancy Modulated Spatial In_2S_3/In_2O_3 Heterojunction. *Adv. Funct. Mater.* **2024**, *34*, 2409031. https://doi.org/10.1002/adfm.202409031.
198. Hirano, T.; Nakade, K.; Li, S.; et al. Chemical etching of a semiconductor surface assisted by single sheets of reduced graphene oxide. *Carbon* **2018**, *127*, 681–687. https://doi.org/10.1016/j.carbon.2017.11.053.
199. Wei, Y.; Zhu, L.; Jia, L.; et al. Study on the Influence of Etchant Composition and Etching Process on the Precision of Stainless-Steel Microchannel and Etching Mechanism. *Adv. Eng. Mater.* **2024**, *26*, 2301731. https://doi.org/10.1002/adem.202301731.
200. Sahoo, G.S.; Tripathy, S.P.; Joshi, D.S.; et al. Microwave induced chemical etching of CR-39 with KOH etchant: Comparison with chemical etching. *Nucl. Instrum. Meth. A* **2019**, *935*, 143–147. https://doi.org/10.1016/j.nima.2019.05.010.
201. Zhu, A.-X.; Dou, A.-N.; Fang, X.-D.; et al. Retracted Article: Chemical etching of a cobalt-based metal-organic framework for enhancing the electrocatalytic oxygen evolution reaction. *J. Mater. Chem. A* **2017**. https://doi.org/10.1039/C7TA02103H.
202. Feng, Y.; Yao, J. Tailoring the structure and function of metal organic framework by chemical etching for diverse applications. *Coord. Chem. Rev.* **2022**, *470*, 214699. https://doi.org/10.1016/j.ccr.2022.214699.

203. Xu, G.; He, Q.; Huang, K.; et al. Hierarchically Ultrasmall Hf-Based MOF: Mesopore Adjustment and Reconstruction by Recycle Using Acid Etching Strategy. *Chem. Eng. J.* **2023**, *455*, 140632. https://doi.org/10.1016/j.cej.2022.140632.
204. Doan, H.V.; Sartbaeva, A.; Eloi, J.-C.; et al. Defective hierarchical porous copper-based metal-organic frameworks synthesised via facile acid etching strategy. *Sci. Rep.* **2019**, *9*, 10887. https://doi.org/10.1038/s41598-019-47314-1.
205. Gao, W.; Chen, D.; Quan, H.; et al. Fabrication of Hierarchical Porous Metal–Organic Framework Electrode for Aqueous Asymmetric Supercapacitor. *ACS Sustain. Chem. Eng.* **2017**, *5*, 4144–4153. https://doi.org/10.1021/acssuschemeng.7b00112.
206. Xiong, W.; Zhao, L.; Ouyang, J.; et al. Surface-modified composites of metal–organic framework and wood-derived carbon for high-performance supercapacitors. *J. Colloid Interface Sci.* **2025**, *679*, 243–252. https://doi.org/10.1016/j.jcis.2024.09.247.
207. Dong, H.; Li, L.; Li, C. Controlled alkali etching of MOFs with secondary building units for low-concentration CO_2 capture. *Chem. Sci.* **2023**, *14*, 8507–8513. https://doi.org/10.1039/D3SC03213B.
208. Li, L.; Yi, J.-D.; Fang, Z.-B.; et al. Creating Giant Secondary Building Layers via Alkali-Etching Exfoliation for Precise Synthesis of Metal–Organic Frameworks. *Chem. Mater.* **2019**, *31*, 7584–7589. https://doi.org/10.1021/acs.chemmater.9b02375.
209. Lu, Z.; Zhu, W.; Lei, X.; et al. High pseudocapacitive cobalt carbonate hydroxide films derived from CoAl layered double hydroxides. *Nanoscale* **2012**, *4*, 3640–3643. https://doi.org/10.1039/C2NR30617D.
210. Yue, P.; Zhang, Y.; Wu, X. Defective ZnCoNiP nanosheets derived from metal-organic-frameworks as electrodes for high-performance supercapacitors. *J. Energy Storage* **2023**, *58*, 106320. https://doi.org/10.1016/j.est.2022.106320.
211. Hassan, H.; Umar, E.; Iqbal, M.W.; et al. Effect of electrolyte optimization on nitrogen-doped MXene ($Ti_3C_2T_x$) coupled with Cu–BTC MOF for a supercapattery and the hydrogen evolution reaction. *New J. Chem.* **2024**, *48*, 6277–6295. https://doi.org/10.1039/D3NJ05510H.
212. Huang, Q.; Hu, L.; Chen, X.; et al. Metal–Organic Framework-Derived N-Doped Carbon with Controllable Mesopore Sizes for Low-Pt Fuel Cells. *Adv. Funct. Mater.* **2023**, *33*, 2302582. https://doi.org/10.1002/adfm.202302582.
213. Feng, L.; Yuan, S.; Zhang, L.-L.; et al. Creating Hierarchical Pores by Controlled Linker Thermolysis in Multivariate Metal–Organic Frameworks. *J. Am. Chem. Soc.* **2018**, *140*, 2363–2372. https://doi.org/10.1021/jacs.7b12916.
214. Chen, J.S.; Sun, X.Y.; Kong, W.Q.; et al. N-doped bimetallic sulfides hollow spheres derived from MOF as battery-type electrode for asymmetric supercapacitors. *J. Energy Storage* **2023**, *73*, 109164. https://doi.org/10.1016/j.est.2023.109164.
215. Aashi; Rani, R.; Alagar, S.; Sharma, J.; et al. Laser-Induced Crafting of Modulated Structural Defects in MOF-Based Supercapacitor for Energy Storage Application. *ACS Mater. Lett.* **2024**, *6*, 1769–1778. https://doi.org/10.1021/acsmaterialslett.4c00206.
216. Cao, X.; Cui, L.; Liu, B.; et al. Reverse synthesis of star anise-like cobalt doped Cu-MOF/$Cu_{2+1}O$ hybrid materials based on a $Cu(OH)_2$ precursor for high performance supercapacitors. *J. Mater. Chem. A* **2019**, *7*, 3815–3827. https://doi.org/10.1039/C8TA11396C.
217. Zheng, K.; Tan, H.; Wang, L.H.; et al. Vertically Oriented $Cu_{2+1}O$@Cu-MOFs Hybrid Clusters for High-Performance Electrochemical Capacitors. *Adv. Mater. Interfaces* **2021**, *8*, 2002145. https://doi.org/10.1002/admi.202002145.
218. Gao, J.; Zhuang, Z.; Zhou, X.; et al. Reversible Mn^{2+}/Mn^{4+} and Mn^{4+}/Mn^{6+} double-electron redoxes in heterostructure $MnS_2/MnSe_2$@HCMs boost high energy storage for hybrid supercapacitors. *Chem. Eng. J.* **2024**, *485*, 149520. https://doi.org/10.1016/j.cej.2024.149520.
219. Wu, Y.-F.; Kuo, T.-R.; Lin, L.-Y.; et al. Investigating energy storage ability of MIL101-(Fe) derivatives prepared using successive carbonization and oxidation for supercapacitors. *J. Energy Storage* **2022**, *55*, 105420. https://doi.org/10.1016/j.est.2022.105420.
220. Su, Y.-Z.; Lin, T.-C.; Tsai, C.-S.; et al. Growth of Metal–Organic Framework within Macroporous PEDOT:PSS Aerogels Prepared by Directional Freezing for Supercapacitors. *ACS Appl. Energy Mater.* **2025**, *8*, 122–133. https://doi.org/10.1021/acsaem.4c02153.
221. Li, J.; Pan, D.; Xu, P.; et al. Rational design of porous nest-like basic Co-Ni carbonates on carbon cloth with optimized electrode process for efficient electrochemical energy storage. *Nano Energy* **2024**, *128*, 109954. https://doi.org/10.1016/j.nanoen.2024.109954.